United States Department of the Interior

GEOLOGICAL SURVEY

Permanent Ground Movement Associated with the 1992 M=7 Cape Mendocino, California, Earthquake: Implications for Damage to Infrastructure and Hazards to Navigation

Ross S. Stein, Grant A. Marshall, Mark H. Murray
U.S. Geological Survey, Menlo Park, California

With Participation by

Emery Balazs, National Geodetic Survey
Gary A. Carver and Thomas A. Dunklin, Humboldt State University
Robert J. McLaughlin, Kirsten Cyr, and Angela Jayko, U.S. Geological Survey

Submitted to

Department of Public Works
County of Humboldt

Funded by

Federal Emergency Management Agency
Governor's Office of Emergency Services, State of California
County of Humboldt, California

FEMA Damage Survey Report No. 080632
"Damage to Vertical Control Monument Network"

U.S. Geological Survey Open-File Report 93-383

Table of Contents

Executive Summary

A critical element of the Humboldt County infrastructure is its vertical control network. The positions of bench marks (BMs) in the network are used for cadastral, roadways, engineering, and flood plain surveys. At the request of the Department of Public Works of Humboldt County, 333 km of the network nearest the 1992 Cape Mendocino earthquake was resurveyed by the National Geodetic Survey in late 1992, with 100 new BMs emplaced. Comparing the new heights with those measured before 1992 gives the vertical deformation associated with the earthquake, which includes motion caused by slip on the earthquake fault, earthquake-triggered surficial disturbances such as landslides and liquefaction, and settling of engineered structures due to earthquake shaking.

We find that 37 BMs in Humboldt County display height changes that can not be accounted for by the earthquake fault slip, and thus indicate monument, soil or structural instability: 18 BMs show subsidence caused by groundwater withdrawal in the Eel River basin; 16 BMs show residual movement of less than a few centimeters, and 4 BMs show major disturbance of up to 4 m. One of the disturbed BMs lies near an earthquake-induced tension crack, and another is near the site of liquefaction in the Salt river bed. Nine of the disturbed BMs are set in bridge abutments or highway overpasses, and 6 are set in retaining walls, and thus might be indicators of structural weakness or incipient failure. In addition, the distribution of landslides, liquefaction, and road cracking reveals other sites of potential ground failure along highways, seawalls, and foundations. Some 1992 BMs could be resurveyed to monitor subsequent movement.

Using a model for the earthquake fault slip that best fits the geodetic and seismic observations of the earthquake, we infer the uplift of shoals and rocks offshore Humboldt County. We estimate that 13 shoals lying in less than 3 fathoms (5.5 m) of water were uplifted by more than 0.45 fathoms (0.83 m), presenting increased hazards to coastal navigation. In addition, a 4 x 8 nautical-mile wide (7 x 14 km) zone is identified as the site of potential seafloor faulting with displacement of up to 3 m, and the head of Mattole Canyon is suggested as the site of possible seafloor landslides. These findings have been furnished to the U.S. Coast Guard for issuance as a Notice to Mariners, and to the National Ocean Survey of NOAA for bathymetric survey planning. We also find that the flood plain boundary of the Mattole river at Petrolia will be shifted by as much as 62 m (200') as a result of the permanent change in elevation caused by the earthquake.

Scheme for Prediction of Earth Movement Associated with the 1992 Cape Mendocino Earthquake

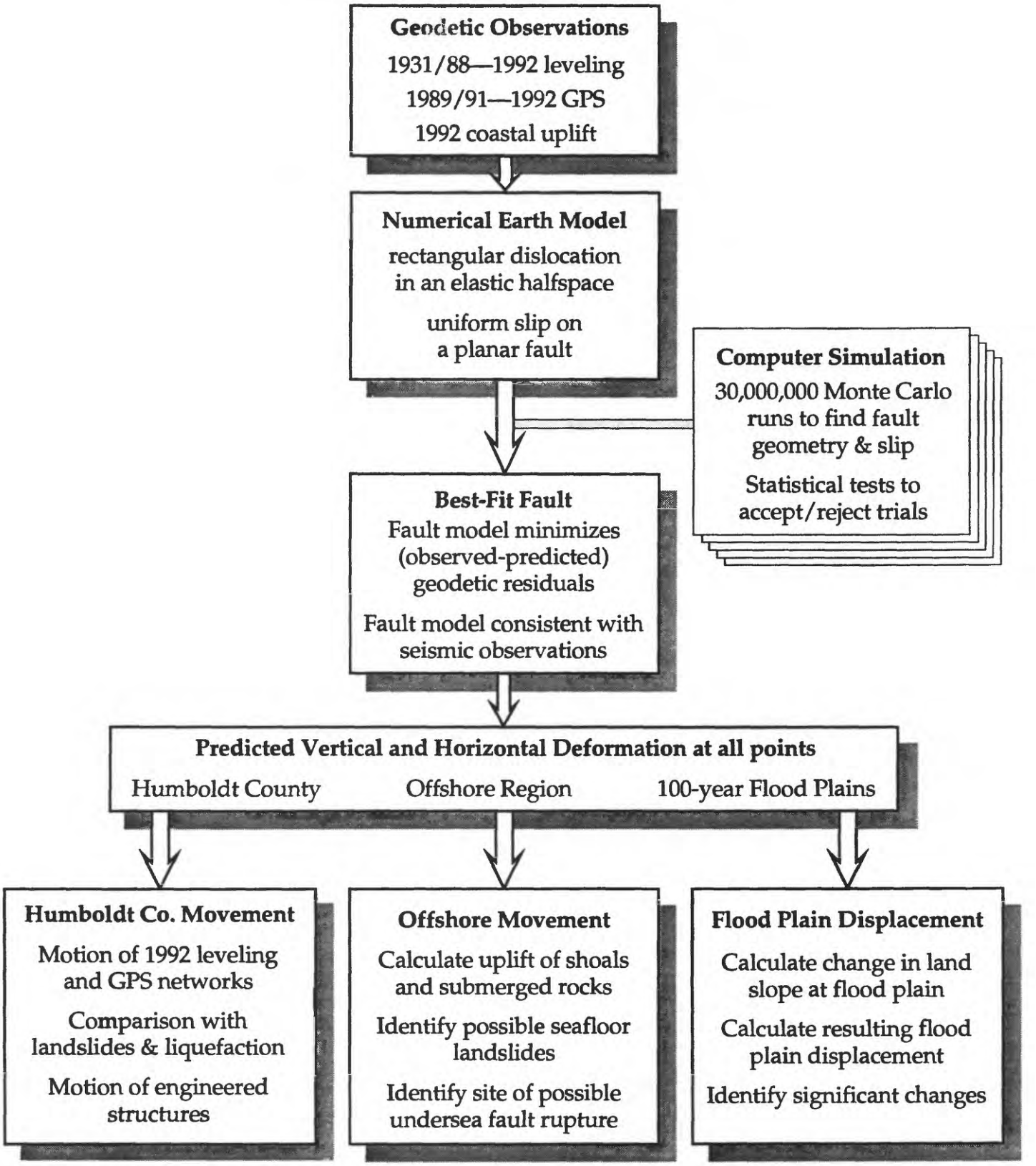

Fig. 1 Strategy followed to predict earthquake deformation in Humboldt County and offshore.

Deformation Modeling Strategy

Goal. We seek to portray or predict the permanent vertical and horizontal deformation that accompanied the 1992 Cape Mendocino earthquake throughout Humboldt County and its offshore extension. Our objective is to predict the displacement of geodetic monuments (leveling bench marks and GPS stations), cultural features (seawalls and roads), natural features (the Eel river flood plain), and hazards to navigation (shoals and submerged rocks). We have, however, no measurements of displacement offshore, and there is only a limited number of horizontal displacement observations (from repeated GPS surveys), and a sparse network of vertical elevation changes (from repeated geodetic leveling and observations of coastal uplift relative to sea level). To overcome this limitation, we determine the deformation field by finding the fault geometry and earthquake slip that are most compatible with the available geodetic and independent seismic observations of the earthquakes. We then use the fault model to predict the deformation everywhere at the earth's surface, both at locations where geodetic observations exist and also where they are absent (Fig. 1).

Modeling Process. We compare displacements predicted for a large number of numerical models of the earthquake faulting to the observed displacements, treating the earthquake fault as a cut or discontinuity embedded in a stiff elastic solid. The fault slip produces strain in the medium and deforms the ground surface. Models which fit the observations within their uncertainties are retained and then winnowed down to those which are also compatible with seismic observations. Thus acceptable model faults must lie close to the mainshock focus, and the earthquake size must be compatible with the earthquake size measured seismically. The best fault model to emerge from this procedure was used to predict the deformation everywhere at the earth's surface.

Global Positioning System Network

Three-dimensional (horizontal and vertical) displacements of 12 GPS (Global Positioning System) monuments within 70 km of the 1992 Cape Mendocino earthquake epicenter, as well as 8 other stations located at greater distances, were determined from surveys conducted by the USGS in 1989, 1991, and one month after the mainshock in 1992 [*Oppenheimer et al*, 1993]. The relative positions of sites near the 1992 epicenter were measured shortly after the 17 August 1991 M=6 Honeydew earthquake, which occurred

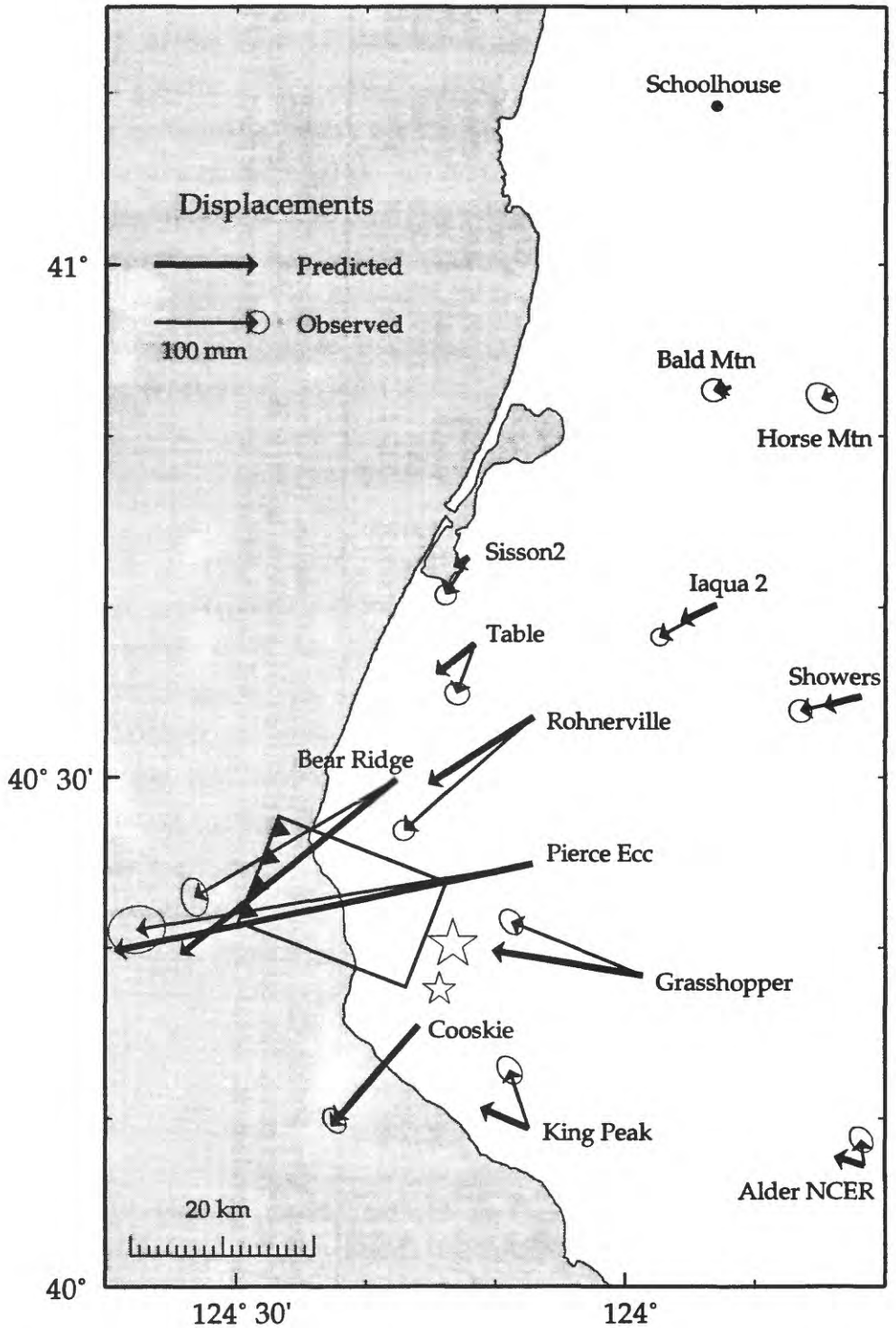

Fig. 2. Horizontal earthquake displacements from the near-field GPS stations with their 95% confidence ellipses. The M=7 Cape Mendocino and M=6 Honeydew mainshocks are shown as stars. The fault model is also shown, with teeth on the upper edge of the thrust fault. Source parameters for the fault model are: dip = 22°SW, centroid depth = 4.2 km, along-strike length = 12.33 km, down-dip width = 21 km, strike = 21°, centroid latitude = N40° 22' 31", centroid longitude = W124° 21' 54", slip = 4.06 m, rake = 129°, moment = 3.16×10^{19} N-m (equivalent to a moment-magnitude **M** = 7.0).

Table 1. GPS Stations used to Find Fault Model

Station	Latitude (° ' ")			Longitude (° ' ")			Elev (m)	North Displacement			East Displacement			Vertical Displacement		
								Obs	Calc	(O-C)	Obs	Calc	(O-C)	Obs	Calc	(O-C)
Pierce eccen.	40	24	58.920	-124	07	11.986	943.13	-0.3867	-0.4013	0.0146	-0.0648	-0.0850	0.0202	-0.1580	-0.0938	-0.0642
Showers	40	34	44.190	-123	41	51.096	1316.05	-0.0595	-0.0332	-0.0263	-0.0141	-0.0086	-0.0055	-0.0216	0.0039	-0.0255
Iaqua 2	40	40	8.289	-123	52	57.424	1107.97	-0.0558	-0.0315	-0.0243	-0.0316	-0.0154	-0.0162	0.0061	0.0007	0.0054
Bald Mtn	40	52	55.228	-123	51	55.449	938.91	-0.0164	-0.0076	-0.0088	-0.0039	-0.0046	0.0007	0.0162	-0.0001	0.0163
Table	40	37	49.059	-124	11	37.380	146.10	-0.0176	-0.0347	0.0171	-0.0481	-0.0292	-0.0189	0.0163	-0.0152	0.0315
Horse Mtn	40	52	29.002	-123	43	58.605	1481.42	-0.0118	-0.0086	-0.0032	-0.0043	-0.0047	0.0004	-0.0205	0.0011	-0.0216
Rohnerville	40	33	31.868	-124	07	7.685	159.44	-0.1268	-0.0990	-0.0278	-0.1101	-0.0648	-0.0453	-0.0152	-0.0167	0.0015
Sisson2	40	42	55.572	-124	12	7.094	132.93	-0.0227	-0.0114	-0.0113	-0.0364	-0.0082	-0.0282	0.0113	-0.0100	0.0213
Alder NCER	40	07	13.036	-123	41	35.404	1156.07	-0.0030	-0.0250	0.0220	0.0253	0.0093	0.0160	0.0022	0.0034	-0.0012
Grasshopper	40	18	22.977	-123	58	40.312	1000.41	-0.1288	-0.1407	0.0119	0.0526	0.0244	0.0282	-0.0362	-0.0064	-0.0298
King Peak	40	09	24.627	-124	07	27.534	1216.20	-0.0184	-0.0412	0.0228	0.0563	0.0179	0.0384	0.0199	-0.0082	0.0281
Cooskie	40	15	24.526	-124	15	57.656	868.49	-0.0823	-0.0750	-0.0073	-0.0920	-0.1070	0.0150	0.0629	0.0588	0.0041
Bear Ridge	40	29	51.724	-124	17	40.122	720.86	-0.1973	-0.2084	0.0111	-0.1139	-0.1748	0.0609	-0.0609	-0.0888	0.0279
Schoolhouse	41	09	12.268	-123	52	55.028	915.56	0	0	0	0	0	0	0	0	0

Notes. Displacements are in meters. 'Obs' is observed; 'Calc' is calculated for the fault model; '(O-C)' is the residual displacement, observed minus calculated. The uncertainty of the vertical displacement (where positive values indicate uplift) is about five times greater than that of the horizontal motion. Displacements are calculated relative to station Schoolhouse, which is held fixed. Station displacements are plotted in Fig. 2.

6 km south of the Cape Mendocino epicenter. The coseismic displacements were measured by subtracting the 1989 positions from the 1992 positions, except near the Honeydew earthquake, where the 1991 observations were used instead of the 1989 survey. The steady deformation not directly related to the earthquakes (the secular strain accumulation) was then removed by using the displacement rate measured by the USGS at these sites by laser Geodolite during 1981-89. The peak horizontal displacement of 40±2 cm was found 13 km northwest of the epicenter (Fig. 2). Some 11 GPS sites displayed horizontal displacement larger than measurement uncertainty; at only three sites was the vertical displacement significant (Table 1).

Coastal Elevation Changes

The uplift of the Mendocino coastline killed marine intertidal flora and fauna that are sensitive to height above sea level. To estimate coseismic elevation change, Carver *et al* [1993] measured the vertical extent of the death of species affixed to the coastal rock outcrops. Mussels, barnacles and seaweed (Pelvetoipsis) gave the most reliable indicators along the 12 coastal points (Fig. 3c). These observations of uplift supplement elevation change measurements furnished by the geodetic leveling network. At each site, we use the mean estimated height change from the three marine intertidal indicators, assigning half the difference in elevation change measured for the mussels and seaweed as the measurement uncertainty. Where only one species is present, we use the mean uncertainty of the redundant observations, 150 mm.

Leveling Network

The vertical deformation associated with the Cape Mendocino earthquake is inferred by subtracting elevations measured during 1931-1988 (Fig. 3a) by the National Geodetic Survey (NGS) from elevations measured during a post-earthquake survey conducted by the NGS during August-October 1992 (Fig. 3b). Bench marks (BMs) common to both periods form the earthquake dataset (Fig. 3c). Corrections for BM motion due to ground water fluctuations were made where feasible, unstable BMs were removed, a subset of BMs were deleted to create a uniform distribution of BMs within the network, and survey precision was assessed to assign uncertainty estimates to each section, or pair of BMs.

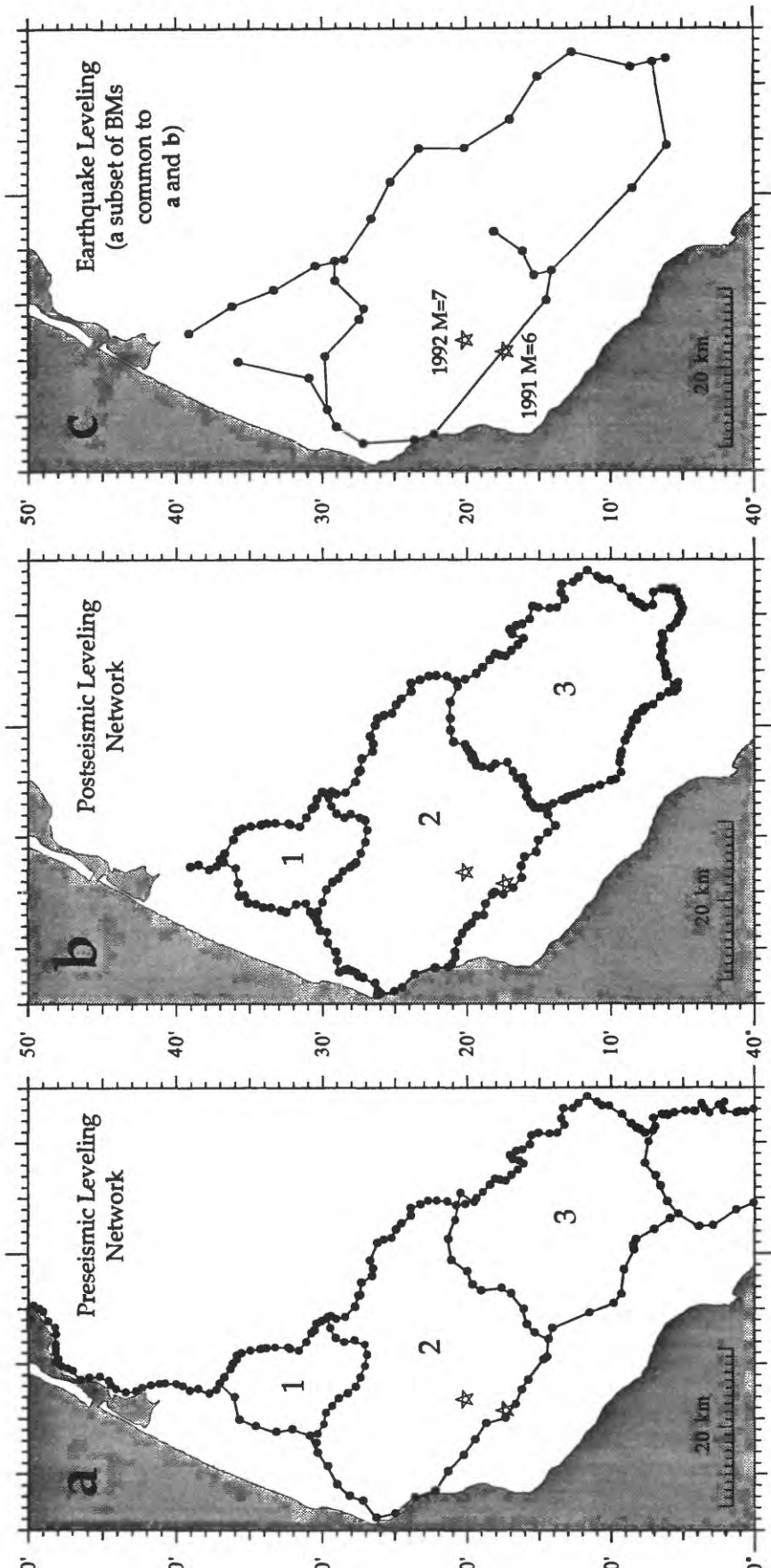

Fig. 3 Earthquake elevation changes are constructed by subtracting heights of bench marks measured after the earthquake (panel b) from heights measured for the common bench marks before the earthquake (panel a). The number of marks along the highway 101 route was then reduced so that the spacing between all bench marks was even. Circuit misclosures are calculated for loops 1, 2, and 3. The loop referred to as 1+2+3 is the large outer loop.

Table 2. Leveling Data

NGS L-number	Date	Order	Class	$\alpha_{F\text{-}B}$ mm/$\sqrt{\text{km}}$	% double-run
Preseismic Data					
L389	11/31	1	II	1.32	99
L4576	02/35	2		3.48	4
L5479	01/35	2		2.18	2
L6711/1	06/35	2		n/a	0
L6711/2	06/35	2		2.03	2
L9851	06/42	2		2.22	33
L21206	08/67	1	II	1.35	100
L25053	10/88	1	II	0.62	20
Postseismic Data					
L25377/1	08/92	1	II	1.21	10
L25377/2	09/92	1	II	1.16	11
L25377/3	10/92	1	II	0.85	11
L25377/4	10/92	1	II	0.93	10

$\alpha = \frac{1}{N}\sum_{j}^{N} \text{s.d.}_j$, where N is the number of double-run sections, and $\text{s.d.}_j = \sqrt{\frac{\text{var}_j}{D_j}}$

where D_j is the length, in kilometers, of the j^{th} double-run section, and $\text{var}_j = \frac{1}{n}\sum_{i}^{n} (\bar{h} - h_i)^2$

where n is the number of runnings of the j^{th} double-run section, and h_i is the observed height of the section, in millimeters, and $\bar{h}$ is the average height of the n runnings.

Table 3. Circuit Misclosures

Circuit	Misclosure (mm)	Circuit Length (km)	α_{miscl} ($mm/\sqrt{km}$)
Preseismic Data			
1	+54.9	68.8	6.6
1†	-23.5	68.8	2.8
2	-31.0	162.6	2.4
2†	+50.2	162.6	3.9
3	-3.5	131.1	0.3
1+2	+23.8	177.4	1.8
1+2+3	+23.3	224.6	1.5
2+3	-34.5	209.7	2.4
(2+3)†	+46.7	209.7	3.2
(2+3)*	-79.5	204.3	5.6
Postseismic Data			
1	+14.4	71.1	1.7
2	-3.0	152.0	0.3
3	+6.5	135.6	0.6
1+2	+10.9	162.4	0.9
1+2+3	+17.2	228.1	1.1
2+3	+2.7	209.4	0.2

All circuit misclosures are computed in a clock-wise direction. †These circuits substitute L9851 (*1942*) for L6711/1 (*1935*). *This circuit substitutes L25053 (*1988*) for L389 (*1931*).

Leveling Error Analysis

Systematic Errors. All surveys were tested for slope-dependent errors associated with miscalibrated leveling rods [*Stein*, 1981], but no significant errors were detected. The 1967 and 1988 surveys were also examined for magnetic-compensator error typical of leveling conducted between 1967 and 1988 with Zeiss Ni1 automatic-compensators [*Ekström et al.* 1991], but none was found. Subsidence due to ground water withdrawal was assessed along the inland route by examining elevation change measured before the earthquake during 1931, 1967 and 1988. BMs in the Eel river basin were found to have risen slightly during 1931-67 and to have subsided at a rate of up to 3.2 mm/yr during 1967-88. Since the subsidence is likely due to ground water withdrawal, and drought conditions continued through 1992, we corrected these coseismic 1988-92 elevation changes by the observed 1967-88 subsidence rate (Fig. 4), assigning a 50% uncertainty to the correction in the numerical modeling. The northernmost BM along the coastal route was deleted, as it lies within the Eel river basin sediments, and we lack a well-constrained subsidence correction for the BM.

Random Errors. Random leveling errors were assessed in two ways. First, the agreement between the forward and backward measurements of the height between BMs where sections were double-run, $\alpha_{F\text{-}B}$, was computed for each survey (Table 2). Then, the misclosure or disagreement in height measured around each leveling circuit, was calculated to find α_{miscl} (Table 3). In the absence of systematic errors, the two estimates of α should be equal, which generally obtains. Since misclosure estimates are made from a larger number of observations, we use the weighted average α_{miscl} of 3.20 mm for the 1935-42 preseismic surveys. Both 1935 and 1942 surveys traversed the line segment common to loops 1 and 2 (Fig. 3a), and they differ by 80 mm. Because the 1942 survey contains more double-run sections, and because misclosures with the 1942 surveys are slightly smaller (compare loops 1 and 2 to loops $1^{\dagger}$ and $2^{\dagger}$ in Table 3), we used the 1942 survey for the preseismic elevations. For the high-quality 1988 preseismic survey, we use α = 0.80 mm. For the postearthquake 1992 surveys, we use α = 0.85 mm, derived from the weighted average α of the three internal circuits (loops 1, 2, 3 in Fig. 3b) and the external loop (1+2+3).

Deletions. Four BMs were removed from the data set submitted to numerical modeling because they showed elevation changes that differed markedly from adjacent marks. This left 22 BMs spaced 9 km apart and 12 marine coastal observations spaced 2.5 km

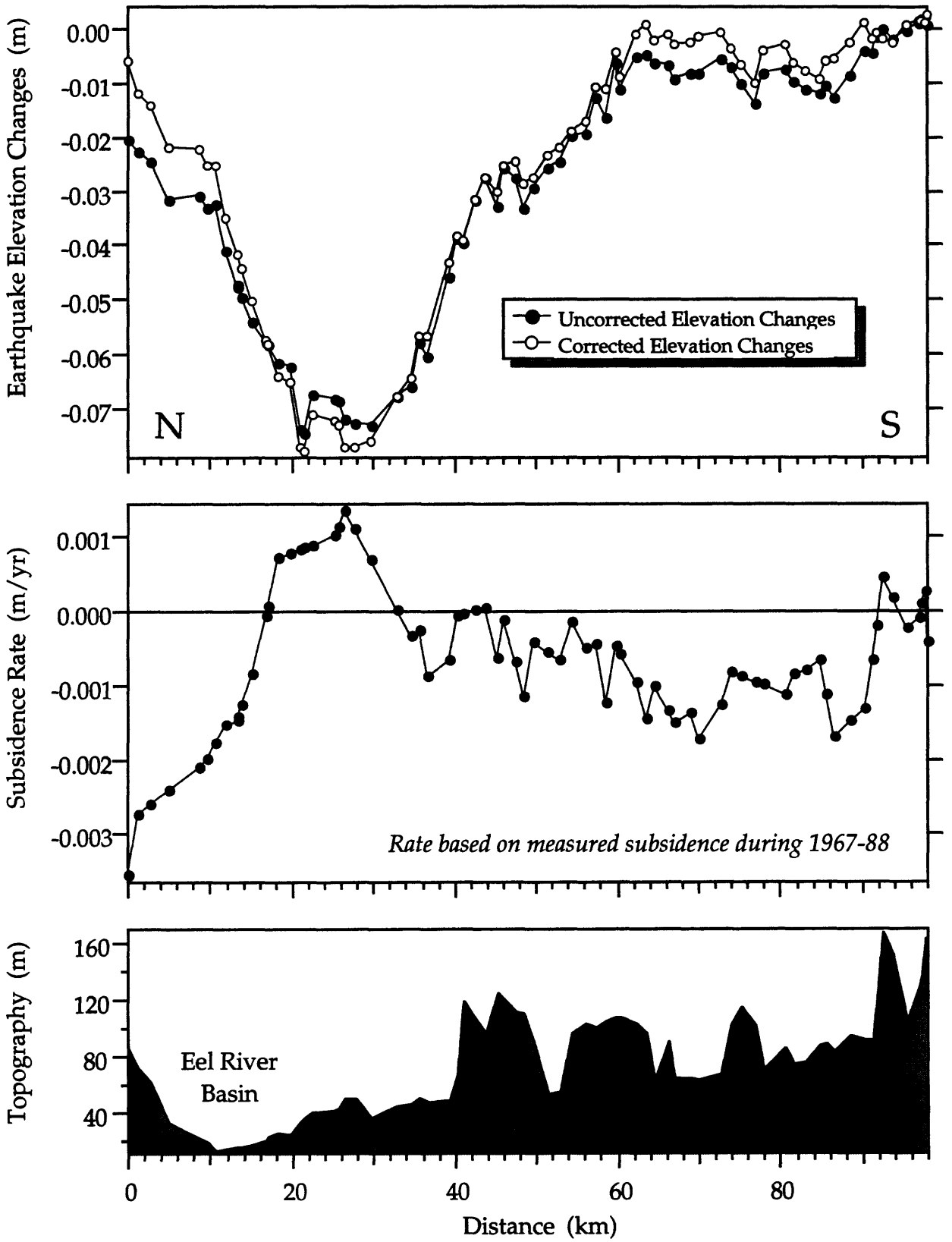

Fig. 4 Profiles of leveling along highway 101. Top panel shows observed and subsidence-corrected elevation change for 1988 to 1992, the earthquake interval. Middle panel shows subsidence rate measured between 1967 and 1988, which is used for the correction. Bottom panel shows route topography.

apart on the western side of the network, where the coseismic elevation change was large, and 74 BMs spaced about 1.5 km apart to the east, where the deformation was modest. Some 5 BMs that lie within 10 km of the 17 August 1991 M=6.2 Honeydew earthquake were also removed, as they recorded up to 15 cm of uplift associated with the 1991 earthquake (Table 5). To avoid having most observations located where the least earthquake deformation occurred, we removed 60 BMs along the eastern route, making the BM spacing roughly uniform throughout the network (Fig. 3c).

Network Signal to Noise. The difference in elevation change measured between successive pairs of adjacent leveling BMs is treated as an independent observation, weighted by its associated uncertainty. Thus for the leveling there is no common reference datum and only relative deformation between BMs is considered (Table 4a). In contrast, each coastal marine observation is an independent measurement of elevation change relative to a sea level datum (Table 4b). The signal to noise ratio of the leveling data alone is about 20; for the coastal data it is about 5. The combined signal to noise ratio of about 14 is quite high for datasets of coseismic elevation change.

Numerical Modeling of the Earthquake Deformation

Modeling Methodology. We treat the earth as an elastic halfspace, a medium with a flat upper surface that extends to infinite depth, and assign elastic modulii (or stiffness) that approximates observed earth behavior. Into this medium we embed an elastic dislocation—a rectangular cut or fault—at a given location with a specified length, width, inclination, and orientation. We then calculate how slip (shear displacement) of the fault will deform the earth's surface. This is equivalent to making a cut inside a stiff block of rubber, displacing the two sides of the cut past each other a fixed amount, and measuring how the surface of the rubber block has deformed as a result of the internal cut. At every point where we have a geodetic observation of the earthquake deformation (vertical or horizontal), we calculate the predicted deformation per meter of slip on the fault. We then find the value of fault slip which minimizes the difference between the predicted and observed surface displacements. The observations are weighted such that the most precise observations carry the most weight, following *Marshall et al* [1991].

A fault model is described by 8 parameters related to its location and orientation. Values for these 8 parameters are drawn at random to test faults with a broad range of

Table 4a. Leveling Used to Find Fault Model

NGS ACRN BM_1	NGS ACRN BM_2	Section Distance (km)	Elev. Change Diff. ($BM_1 - BM_2$) (mm)	Error σ (mm)	Signal/Noise S/N
LV0250	LV0239	8.60	16.38	4.49	3.6
LV0239	LV0233	6.57	28.08	3.89	7.2
LV0233	LV0668	7.39	20.68	4.74	4.4
LV0668	LV0670	5.16	5.92	2.69	2.2
LV0670	LV0430	6.96	-12.47	4.24	2.9
LV0430	LU1875	6.49	-25.33	3.05	8.3
LU1875	LU1876	6.29	-14.63	3.21	4.6
LU1876	LU1309	6.93	-5.69	3.26	1.7
LU1309	LU1299	8.03	-17.84	3.68	4.8
LU1299	LU1286	10.26	-0.68	3.80	0.2
LU1286	LU1275	7.91	2.42	3.30	0.7
LU1275	LU1267	9.80	-4.04	3.68	1.1
LU1267	LU1255	7.27	-0.09	4.46	0.0
LV0382	LV0379	5.86	21.09	8.01	2.6
LV0379	LV0369	28.25	-770.91	17.60	43.8
LV0369	LV0368	2.75	83.40	5.49	15.2
LV0368	LV0365	9.30	1018.29	10.09	100.9
LV0365	LV0363	6.28	-168.01	8.30	20.2
LV0363	LV0362	3.15	112.57	5.87	19.2
LV0362	LV0410	9.67	-35.28	10.30	3.4
LV0410	LV0405	7.09	-9.25	8.81	1.0
LV0405	LV0404	1.52	-38.62	4.09	9.4
LV0404	LV0399	7.68	-80.48	9.18	8.8
LV0399	LV0393	4.29	3.03	6.86	0.4
LU1262	LU1472	20.72	-11.99	15.07	0.8
LU1472	LU1477	13.13	-27.16	12.00	2.3
LV0362	LV0220	6.33	-113.97	8.33	13.7

Overall signal-to-noise ratio 22.5

Signal-to-noise ratio's are calculated with $S/N = \frac{|\text{Elevation Change}|}{\text{Error}}$ Overall signal-to-noise is calculated as $S/N = \sqrt{\frac{1}{N}\sum_{i}^{N}\left(\frac{\Delta H_i}{\sigma_i}\right)^2}$ where ΔH_i is the coseismic elevation change of the section, σ_i is the error for that section, and N is the number of sections.

Table 4b. Coastal Elevation Changes Used to Find Fault Model

Observation Site	Elevation Change ΔH (mm)	Uncertainty σ (mm)	Signal/Noise Ratio
Bear River Ridge	0	150	0.0
Cape Mendocino	670	100	6.7
Steam Boat Rock	900	150	6.0
Devils Gate	960	100	9.6
Mussel Rock	1,470	220	6.7
Seal Lion Rock	990	180	5.5
Mattole Point	810	150	5.4
South of Mattole Point	710	190	3.7
Fourmile Creek	380	60	6.3
Lighthouse	310	150	2.1
Sea Lion Gulch	0	150	0.0
Cooskie Creek	0	150	0.0
Overall signal-to-noise ratio 5.3			

Note: observation sites do not have permanent monuments, and place names vary on different maps. Use the latitude and longitude in Table 5 to locate observation sites.

geometries and positions, an approach known as the Monte Carlo procedure. In each test, the model residuals are compared to an estimate of the maximum tolerable residual consistent with the observations. The maximum is based on the number of parameters in the model, the number of observations, their associated uncertainties. Models that satisfy this criterion are saved; unsuccessful models are discarded. Out of 30 million models tested on a Sun computer, about 1,000 satisfied the data. The distribution of successful models furnishes an estimate of the uncertainty in the fault location, orientation, and slip. The single model which best predicted the observed surface deformation was then used to calculate the deformation at all points, including sites where we lack geodetic observations, such as regions far from the leveling or GPS networks (Map A) and offshore (Map B). The observed and predicted changes for this model are listed in Tables 1 and 5.

Best-Fitting Model. To check that the fault model inferred solely from the geodetic data is sound, we compared the model to independent seismic observations. The M=7 mainshock epicenter lies at the base of the model fault, and the sides of the model fault are lined by aftershocks. In addition, the inclination of the model fault and its direction of slip are close to that found from seismic observations. (The 2 largest aftershocks, however, lie 10 km west of the model fault at significantly greater depth. These shocks appear to have struck on separate faults.) The upper edge of the model fault lies several kilometers below the seafloor, 1-10 km west of the coastline between Cape Mendocino and Punta Gorda. This explains why major surface faulting was not observed in Humboldt County. Although it is not known whether the fault ruptured the seafloor, it is likely that upwarping and some disturbance of the seafloor took place.

Disturbed Bench Marks and Structures in Humboldt County

Deformation Caused by Slip on the Earthquake Fault. Most of the movement of the 105 BMs for which there is a pre- and post-earthquake survey is attributable to slip on the earthquake fault. The residual deformation (observed minus predicted elevation change in Table 5) is largest for 37 BMs and 2 sites of coastal uplift. The BMs with high residuals are candidates for settling caused by long-term groundwater withdrawal, and for disturbance by earthquake shaking, landslides, and liquefaction (Table 6). Note that such a list could not have been compiled had we not removed the movement associated with the earthquake fault slip, because the elevation change caused by the fault slip (up

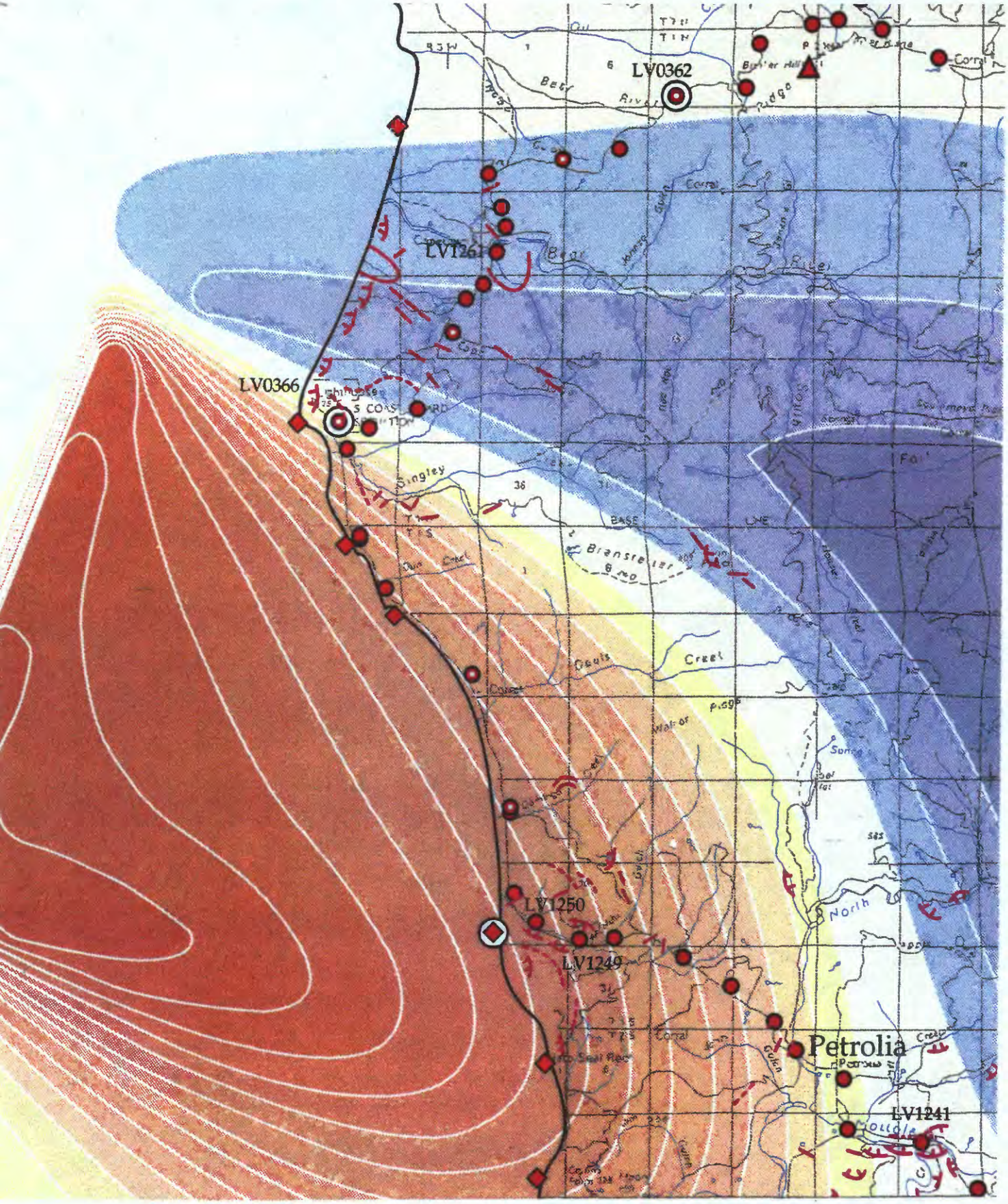

Fig. 5. Leveling network in the Cape Mendocino area affected by the 1992 earthquake (from Map A). Red dots are BMs surveyed in 1992; red dots with white center dot were also surveyed before 1992; white-encircled red dots are BMs identified as unstable or disturbed in Table 6; coastal uplift was measured by *Carver* et al [1994] at red diamonds. Magenta lines are sites of earthquake-induced landslides, tension cracks, ridge spreading, and liquefaction from *Dunklin* [1992]; graded colors indicate earthquake uplift (brown) and subsidence (blue).

Table 5. Observed and Predicted Earthquake Elevation Changes

NGS ACRN	Stamped Designation	Latitude dd/mm/ss	Longitude ddd/mm/ss	Obs (mm)	Pred (mm)	(Obs - Pred) (mm)
L25377/1, L25053						
LV0250	G 1087 RESET	40 39 7	124 12 36	-8.9	-8.7	-0.2
LV0248	F 1087	40 38 33	124 12 27	-11.2	-9.3	-1.9
LV0659	L 1401	40 37 46	124 12 52	-13.0	-11.1	-1.9
LV0243	C 1087 RESET	40 37 2	124 11 55	-20.4	-11.2	-9.2
LV0239	Z 1086	40 36 7	124 10 9	-19.5	-10.4	-9.1
LV0238	K 100	40 35 51	124 9 27	-21.9	-9.8	-12.1
LV0237	Y 1086	40 35 32	124 9 12	-21.1	-10.0	-11.1
LV0236	X 1086	40 34 56	124 8 59	-29.6	-11.0	-18.6
LV0234	W 1086	40 34 15	124 8 53	-36.2	-12.6	-23.6
LV0235	L 100	40 34 9	124 8 47	-36.0	-12.7	-23.3
LV0660	M 1401	40 33 48	124 8 43	-38.1	-13.7	-24.4
LV0233	V 1086	40 33 13	124 8 40	-42.6	-15.7	-26.9
LV0231	N 100	40 32 19	124 8 41	-46.2	-19.9	-26.3
LV0664	P 1401	40 32 12	124 8 48	-46.6	-20.9	-25.7
LV0229	T 1086	40 31 34	124 8 59	-50.0	-25.6	-24.4
LV0665	Q 1401	40 31 4	124 8 13	-50.9	-25.9	-25.0
LV0666	S 1401	40 30 42	124 7 24	-62.6	-24.6	-38.0
LV0667	R 1401	40 30 30	124 7 8	-63.2	-24.6	-38.6
LV0668	T 1401	40 30 20	124 6 30	-56.2	-22.5	-33.7
LV0395	Q 1086	40 29 40	124 6 4	-56.9	-24.4	-32.5
LV0669	U 1401	40 29 19	124 5 51	-57.2	-25.4	-31.8
LV0393	S 100	40 28 59	124 6 4	-60.5	-29.2	-31.3
LV0670	V 1401	40 28 22	124 5 54	-61.3	-32.6	-28.7
LV0671	W 1401	40 27 41	124 4 58	-61.9	-29.6	-32.3
LV0433	L 1086	40 27 26	124 3 59	-94.0	-23.3	-70.7
LV0672	X 1401	40 27 19	124 3 52	-153.3	-23.0	-130.3
LV0673	Y 1401	40 27 14	124 2 48	-56.5	-16.4	-40.1
LV0430	H 1086	40 26 29	124 2 11	-54.7	-14.9	-39.8
LV0429	G 1086	40 26 25	124 1 30	-46.3	-11.4	-34.9
LV0428	HWY 101 STA 477+00 POC	40 26 38	124 0 48	-48.9	-7.8	-41.1
LU1490	E 1086	40 26 6	123 59 13	-34.6	-2.7	-31.9
LU1489	D 1086	40 25 41	123 58 56	-27.5	-2.2	-25.3
LU1875	Z 1401	40 25 9	123 58 46	-28.1	-2.0	-26.1
LU1487	B 1086	40 24 50	123 57 59	-20.3	0.0	-20.3
LU1486	A 1086	40 24 28	123 57 26	-16.1	1.2	-17.3
LU1485	Z 1085	40 23 50	123 56 47	-21.2	2.5	-23.7
LU1484	Y 1085	40 23 49	123 56 5	-14.4	3.8	-18.2
LU1876	A 1404 X	40 23 11	123 55 45	-16.0	4.3	-20.3
LU1482	W 1085	40 22 37	123 55 25	-21.8	4.8	-26.6
LU1481	V 1085	40 22 4	123 55 24	-18.1	4.8	-22.9
LU1877	B 1404 X	40 21 19	123 55 27	-14.2	4.8	-19.0
LU1310	T 1085	40 20 41	123 55 51	-13.1	4.3	-17.4
LU1309	S 1085	40 20 4	123 55 43	-8.2	4.6	-12.8
LU1307	R 1085	40 19 18	123 55 12	-7.8	5.5	-13.3

Table 5. continued

NGS ACRN	Stamped Designation	Latitude dd/mm/ss	Longitude ddd/mm/ss	Obs (mm)	Pred (mm)	(Obs - Pred) (mm)
LU1306	Q 1085	40 18 49	123 54 39	-1.1	6.2	-7.3
LU1304	P 1085	40 18 19	123 53 59	-4.9	6.9	-11.8
LU1303	N 1085	40 17 57	123 53 27	5.0	7.4	-2.4
LU1302	M 1085	40 17 39	123 53 33	0.3	7.3	-7.0
LU1301	L 1085	40 17 15	123 53 38	15.9	7.3	8.6
LU1299	K 1085	40 16 51	123 53 8	6.4	7.7	-1.3
LU1298	J 1085	40 16 24	123 52 39	6.5	8.0	-1.5
LU1295	H 1085	40 16 0	123 52 6	5.0	8.3	-3.3
LU1293	F 1085	40 16 45	123 51 42	4.8	8.5	-3.7
LU1292	E 1085	40 16 56	123 51 20	2.3	8.7	-6.4
LU1291	H 101	40 16 29	123 50 58	-4.9	8.8	-13.7
LU1290	D 1085	40 16 4	123 50 50	3.4	8.8	-5.4
LU1289	J 101	40 15 33	123 50 22	3.3	8.9	-5.6
LU1286	B 1085	40 14 57	123 49 18	5.8	9.2	-3.4
LU1284	A 1085	40 14 13	123 49 22	4.4	9.1	-4.7
LU1879	D 1404 X	40 13 40	123 49 18	1.3	9.0	-7.7
LU1280	X 1084	40 13 10	123 48 35	-2.4	9.1	-11.5
LU1279	A 634	40 13 24	123 47 59	3.5	9.3	-5.8
LU1275	W 1084	40 12 35	123 47 4	4.0	9.3	-5.3
LU1274	V 1084	40 12 12	123 46 36	1.8	9.3	-7.5
LU1272	U 1084	40 11 35	123 45 58	0.3	9.3	-9.0
LU1271	T 1084	40 10 55	123 46 29	-0.6	9.1	-9.7
LU1880	E 1404	40 10 33	123 46 48	0.9	9.0	-8.1
LU1270	S 1084	40 10 4	123 46 50	-1.1	8.9	-10.0
LU1881	F 1404	40 9 10	123 47 37	3.0	8.6	-5.6
LU1267	P 1084	40 8 31	123 48 24	7.3	8.3	-1.0
LU1266	N 1084	40 8 8	123 48 51	6.9	8.1	-1.2
LU1265	M 1084	40 7 53	123 48 59	9.9	8.0	1.9
LU1264	L 1084	40 7 34	123 49 19	11.6	7.9	3.7
LU1882	G 1404	40 7 2	123 49 7	9.6	7.8	1.8
LU1262	W 101	40 6 59	123 47 57	11.2	8.0	3.2
LU1259	X 101 RESET	40 6 24	123 47 38	12.5	8.0	4.5
LU1257	G 1084	40 6 21	123 47 39	13.3	8.0	5.3
LU1255	XX 101	40 6 4	123 47 37	13.7	8.0	5.7
LU1254	F 1084	40 5 59	123 47 43	12.5	8.0	4.5
L25377/2, L4576, L5479, L6711/2						
LU1262	W 101	40 6 59	123 47 57	11.2	8.0	3.2
* LU1472	J 227	40 6 0	123 55 27	23.2	5.7	17.5
* LU1477	J 230	40 8 23	123 59 23	50.4	3.7	46.7
* LV0382	B 230	40 13 58	124 6 55	162.4	-15.1	177.5
* LV0427	Y 268	40 15 13	124 7 20	137.2	-25.1	162.3
* LV0425	W 268	40 16 0	124 5 11	68.9	-20.4	89.3
LV0423	U 268	40 17 59	124 3 21	-1.1	-19.5	18.4

Table 5. concluded

NGS ACRN	Stamped Designation	Latitude dd/mm/ss	Longitude ddd/mm/ss	Obs (mm)	Pred (mm)	(Obs - Pred) (mm)
L25377/3, L9851, L5479, L6711/1						
LV0382	B 230	40 13 58	124 6 55	162.4	-15.1	177.5
LV0379	Z 229	40 14 21	124 9 34	135.8	-23.0	158.8
LV0369	Q 229	40 22 9	124 21 40	880.0	815.2	64.8
LV0368	P 229	40 23 32	124 22 13	794.0	723.2	70.8
LV0366	M 229	40 26 10	124 24 3	-3476.0	301.6	-3777.6
LV0365	L 229	40 27 6	124 22 29	-233.1	-268.8	35.7
LV0363	J 229	40 28 54	124 21 1	-71.0	-111.1	40.1
LV0362	H 229	40 29 34	124 19 26	-186.5	-90.1	-96.4
LV0410	K 275	40 29 42	124 14 39	-166.4	-83.3	-83.1
LV0406	H 275	40 27 39	124 12 15	-232.0	-140.8	-91.2
LV0405	R 649	40 27 19	124 11 23	-163.9	-137.8	-26.1
LV0404	G 275	40 27 1	124 10 22	-126.7	-125.4	-1.3
LV0402	F 275	40 27 1	124 8 25	-2034.7	-82.7	-1952.0
LV0399	N 649	40 29 0	124 7 50	-53.5	-43.6	-9.9
LV0393	S 100	40 28 59	124 6 4	-60.5	-29.6	-30.9
L25377/4, L5479						
LV0362	H229	40 29 34	124 19 26	-186.5	-90.1	-96.4
LV0220	F229	40 30 49	124 16 39	-72.5	-61.0	-11.5
LV0217	B229	40 35 41	124 15 13	-227.6	-19.7	-207.9
Coastal Uplift (no permanent BMs)						
Bear River Ridge		40 29 16	124 23 13	0.0	-96.6	96.6
Cape Mendocino		40 26 10	124 24 26	670.0	429.4	240.6
Steam Boat Rock		40 24 55	124 23 45	900.0	720.4	179.6
Devils Gate		40 24 12	124 23 6	960.0	747.3	212.7
Mussel Rock		40 20 51	124 21 54	1470.0	961.7	508.3
Sea Lion Rock		40 19 29	124 20 59	990.0	881.1	108.9
Mattole Point		40 18 17	124 21 10	810.0	722.7	87.3
South Mattole Point		40 16 36	124 21 45	710.0	349.2	360.8
Fourmile Creek		40 15 22	124 21 24	380.0	186.4	193.6
Lighthouse		40 14 54	124 20 55	310.0	147.6	162.4
Sea Lion Gulch		40 14 23	124 19 50	0.0	109.7	-109.7
Cooskie Creek		40 12 15	124 18 11	0.0	23.6	-23.6

* These bench marks are also affected by the 17 August 1991 M=6 Honeydew earthquake, and thus their residual deformation is larger than predicted for the Cape Mendocino earthquake alone.

Table 6. Disturbed Bench Marks

Stamped Designation	NGS ACRN	Disturbance Type	Mark Type (year)	(Obs - Pred) (mm)
G 1087 RESET	LV0250	ground water withdrawal	†	-0.2
F 1087	LV0248	ground water withdrawal	†	-1.9
L 1401	LV0659	ground water withdrawal	†	-1.9
C 1087 RESET	LV0243	g/w + minor disturbance	culvert headwall 1970	-9.2
Z 1086	LV0239	ground water withdrawal	†	-9.1
K 100	LV0238	ground water withdrawal	†	-12.1
Y 1086	LV0237	g/w + minor disturbance	culvert headwall 1967	-11.1
X 1086	LV0236	ground water withdrawal	†	-18.6
W 1086	LV0234	g/w + minor disturbance	culvert headwall 1967	-23.6
L 100	LV0235	ground water withdrawal	†	-23.3
M 1401	LV0660	ground water withdrawal	†	-24.4
V 1086	LV0233	ground water withdrawal	†	-26.9
N 100	LV0231	ground water withdrawal	†	-26.3
P 1401	LV0664	ground water withdrawal	†	-25.7
T 1086	LV0229	ground water withdrawal	†	-24.4
Q 1401	LV0665	ground water withdrawal	†	-25.0
S 1401	LV0666	ground water + disturbed	bridge abutment 1988	-38.0
R 1401	LV0667	ground water + disturbed	bridge abutment 1988	-38.6
T 1401	LV0668	ground water withdrawal	†	-33.7
Q 1086	LV0395	ground water withdrawal	†	-32.5
U 1401	LV0669	ground water withdrawal	†	-31.8
S 100	LV0393	ground water withdrawal	†	-31.3
G 1086	LV0429	minor disturbance	bridge guardrail 1967	-34.9
L 1086	LV0433	major disturbance	bridge abutment 1967	-70.7
X 1401	LV0672	major disturbance	bridge abutment 1988	-130.3
L 1085	LU1301	minor disturbance	retaining wall 1967	8.6
W 1085	LU1482	minor disturbance	overpass headwall 1967	-26.6
Z 1085	LU1485	minor disturbance	bridge guardrail 1967	-23.7
P 1085	LU1304	minor disturbance	bridge pier 1967	-11.8
M 1085	LU1302	minor disturbance	bridge abutment 1967	-7.0
X 1084	LU1280	minor disturbance	culvert headwall 1967	-11.5
S 1084	LU1270	minor disturbance	culvert headwall 1967	-10.0
H 101	LU1291	minor disturbance	concrete post 1931	-13.7
M 229	LV0366	major disturbance	concrete post 1935	-3777.6
F 275	LV0402	major disturbance	concrete post 1935	-1952.0
H229	LV0362	minor disturbance	concrete post 1935	-96.4
B229	LV0217	ground water withdrawal	†	-207.9
Mussel Rock		major disturbance	(no bench mark)	508.3
So. of Mattole Pt.		minor disturbance	(no bench mark)	360.8

† Mark type is not relevant to subsidence caused by groundwater withdrawal. See Table 5 for latitude and longitude of Bench Marks. (Obs-Pred) is the amount of calculated disturbance, in mm. Negative numbers represent subsidence; positive numbers indicate uplift.

to 1 m) is often larger than the disturbance associated with earthquake shaking, which can be recognized along Highway 101 when it is as small as 1 cm. Some 18 BMs also show subsidence caused by groundwater withdrawal in the Eel River basin, which was verified by examining subsidence during 1967-88 preceding the earthquake.

Earthquake Shaking, Landslides, and Liquefaction. We identify 16 BMs as settling less than a few centimeters. Four BMs show major disturbances of about 10 cm to as much as 4 m (Table 6). Disturbed bench mark LV0366, which subsided 3.7 m, lies close to a major earthquake-induced tension crack, while LV0217 lies next to a site of liquefaction in the Salt River basin (Map A). Nine of the 27 disturbed BMs are set in bridge abutments or highway overpasses, and 6 are set in retaining walls, and thus might be candidates for structural failure. The disturbed marks are indicated in Map A; their NGS bench mark descriptions are listed in Appendix A. In addition, the mapped distribution of landslides, liquefaction, and road cracking from *Dunklin* [1992] in Map A reveals other sites of potential failure along highways and, seawalls, and foundations. For example, BMs LV1261, BMs LV1250, LV1240, and LV1241, all installed by the NGS in 1992 lie near or within debris flows or landslides. These BMs are thus likely to be unstable following winter rains or aftershocks in the near future (see Map A).

Estimated Offshore Deformation

Uplift of Shoals and Submerged Rocks. The predicted vertical deformation offshore Humboldt County is shown in Fig. 6 and Map B. The peak uplift of about 0.7 fathoms (1.3 m) lies 2.5-6 nautical miles (4.5-11 km) west of the coastline between Cape Mendocino and Punta Gorda. Submerged rocks and shoals are estimated to be uplifted as much as 1 m throughout this region. Near Cape Mendocino the predicted deformation gradients are high, with the result that Fauntleroy Rock is estimated to be uplifted by 0.55 fathoms, whereas 1 nautical mile to the northwest, Blunts Reef and The Great Break are unchanged from their pre-earthquake elevations (Fig. 6a). In general, the southern flank of the Cape Mendocino shelf was uplifted the most by the earthquake, with all rocks now 0.45 fathoms (0.8 m) higher relative to sea level. In contrast, Off Rock, Twin Rocks, and Sharp Rock north of the Cape are estimated to have dropped 0.1 fathom as a result of the earthquake. Between Cape Mendocino and the Mattole River, the exposed and submerged rocks do not extend as far offshore. There, Mussel Rocks, The Brothers, and Sea Lion Rock were all uplifted by at least 0.45 fathoms, while

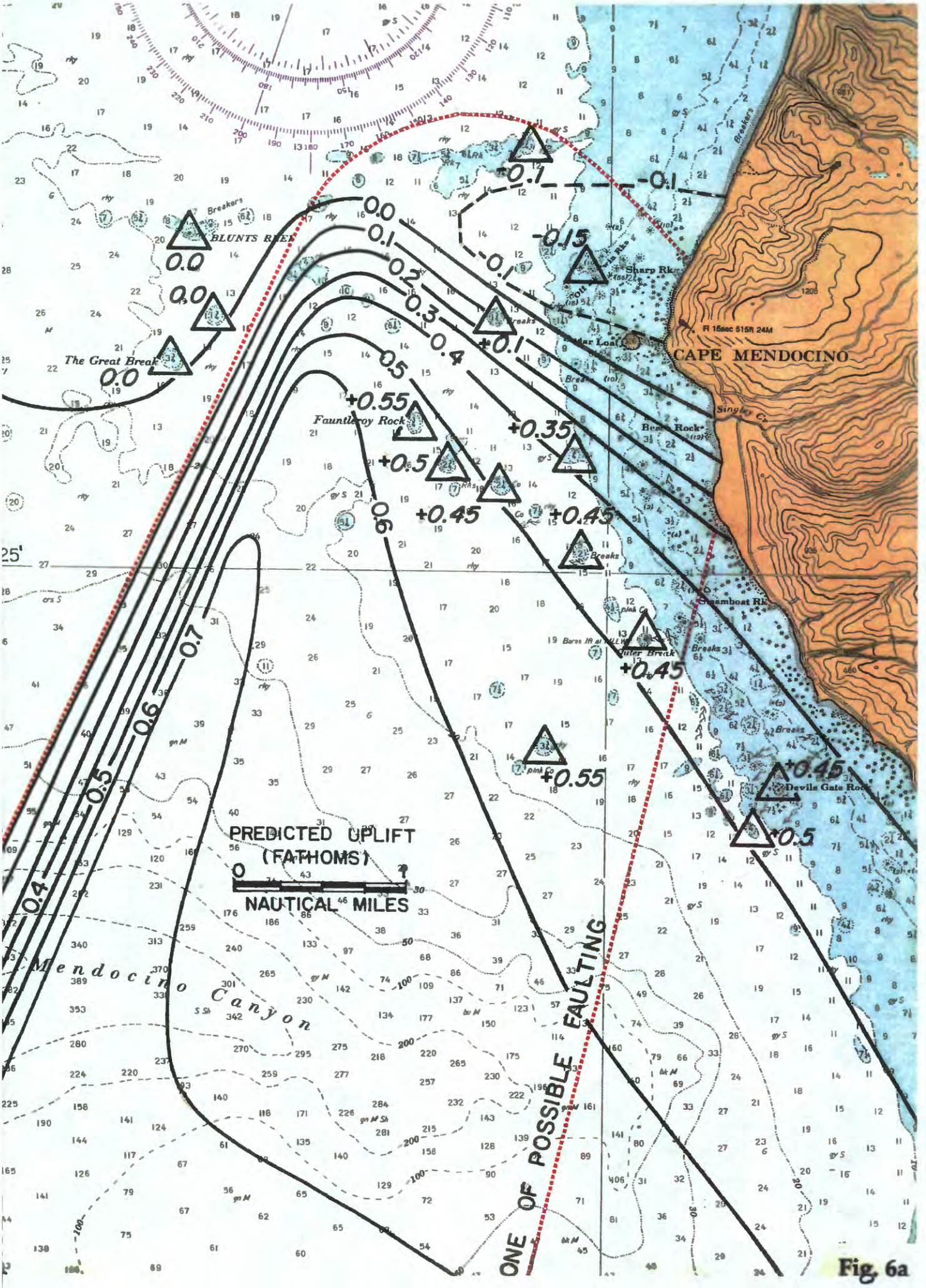
CAPE MENDOCINO
BLUNTS REEF
The Great Break
Fauntleroy Rock
Sharp Rk
Outer Loaf
Beale Rock
Steamboat Rk
Outer Break
Devils Gate Rock
Mendocino Canyon
PREDICTED UPLIFT
(FATHOMS)
NAUTICAL MILES
ONE OF POSSIBLE FAULTING
-0.1
-0.15
0.0
0.1
0.2
0.3
0.4
0.5
0.6
0.7
+0.1
+0.35
+0.45
+0.55

Fig. 6a

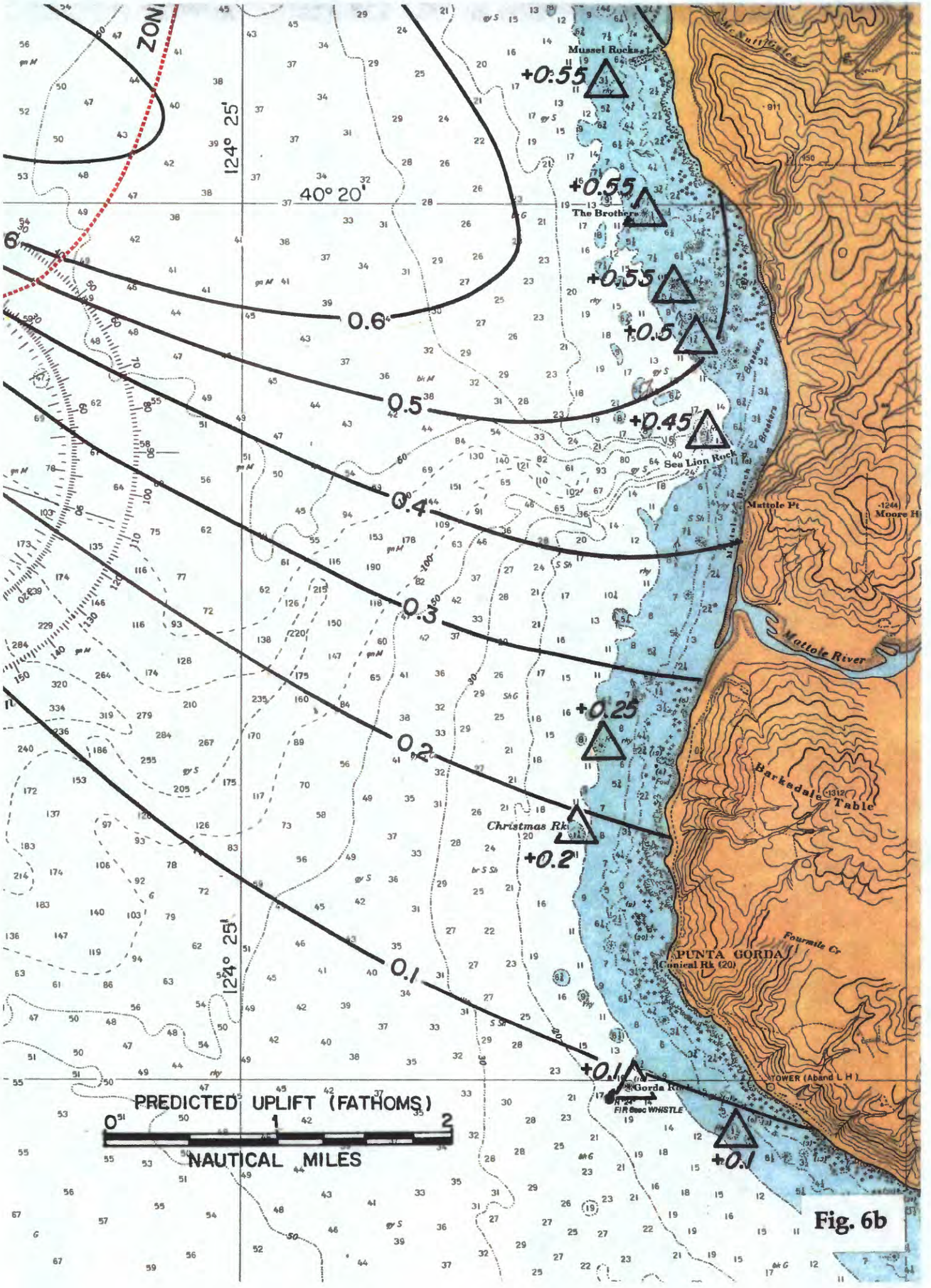
124° 25'
40° 20'
124° 25'
0.6
0.5
0.4
0.3
0.2
0.1
+0.55
+0.55
+0.55
+0.5
+0.45
+0.25
+0.2
+0.1
+0.1
Mussel Rocks
The Brothers
Sea Lion Rock
Mattole Pt
Moore H
Mattole River
Barkedale Table
Christmas Rk
PUNTA GORDA
Conical Rk (20)
Fourmile Cr
Gorda Rock
TOWER (Aband L H)
FIR Sec WHISTLE
PREDICTED UPLIFT (FATHOMS)
0
1
2
NAUTICAL MILES

Fig. 6b

the rocks and reefs near Punta Gorda, such as Christmas Rock, were slightly uplifted (Fig. 6b). The high deformation gradients seen near the Cape make the uplift estimates there less reliable than those to the south. Thus accurate sea level measurements on the rocks by NOAA would enhance the reliability of the predictions near Cape Mendocino.

Table 7. Estimated Motion of Submerged Rocks and Shoals

Rock or Shoal Name ($N \rightarrow S$)	Predicted Uplift (*fathoms*)	Uncertainty (*fathoms*)
Blunts Reef	0.00	±0.15
The Great Break	0.00	±0.15
Fauntelroy Rock	0.55	±0.25
Off Rock	-0.15	±0.10
Twin Rock	-0.15	±0.10
Sharp Rock	-0.15	±0.10
Outer Break	0.45	±0.10
Devils Gate Rock	0.45	±0.10
Mussel Rocks	0.55	±0.10
The Brothers	0.55	±0.10
Sea Lion Rock	0.45	±0.10
Christmas Rock	0.20	±0.05
Gorda Rock	0.10	±0.05

Potential Sites of Submarine Faulting, Folding, and Landslides. The fault model for the Cape Mendocino earthquake does not reach the earth's surface. In other words, the fault may well be hidden from surface inspection. However, the model fault lies about 1 km below the seafloor, and the uncertainty on this depth is several kilometers. Thus it is quite possible that continuous or distributed faulting, with scarps offset by several meters lie offshore. The likely location of such faulting (at the 95% statistical confidence-level) is indicated by the region enclosed by the dotted line in Fig. 6 and Map B. Geologists have found no evidence for faulting at Cape Mendocino, which is the only site where the potential fault zone lies onshore. In addition, submarine landslides are often triggered by large undersea or coastal earthquakes. Such landslides can involve large volumes of seafloor sediments, and may occur in the steep submarine canyons. There is one report by fishermen of possible landsliding in the mouth of Mattole Canyon, based on changes in the bathymetry detected by depth sounding.

Change in Flood Plain Boundaries

Estimation Methodology. To study how the earthquake will alter the boundaries of flood plains in Humboldt County defined by the Flood Boundary and Floodway maps of the National Flood Insurance Program administered by FEMA, we undertook a series of

calculations. We calculate the topographic slope along the edge of the flood plain, and calculate the slope change caused by slip on the Fault Model to obtain the new topographic gradient. Then we calculate the change in position of the flood plain boundary for a flood surface at the same elevation.

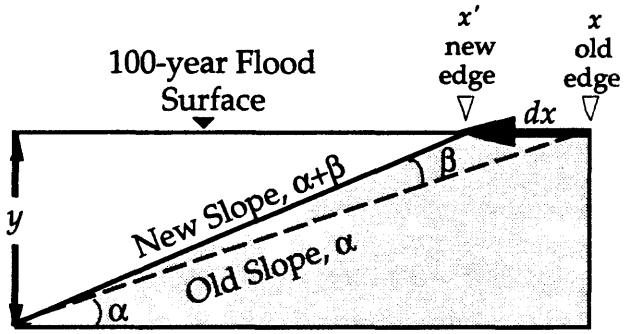

If α is original topographic slope, β is the permanent slope change caused by the earthquake, y is height of the flood plain above sea level, and x is preseismic and x' is postseismic position of flood plain edge, then dx, the change in position of the flood plain boundary, becomes

$$dx = x - x' = y\left(\frac{1}{\tan\alpha} - \frac{1}{\tan(\alpha+\beta)}\right)$$

Thus the earthquake will have the greatest effect in changing the flood plain boundary where the topographic slope is most gentle and the gradient in the vertical earthquake deformation is greatest.

Sites where the Flood Plain is Most Altered. The greatest deformation gradients occur near the coastline from Cape Mendocino to Punta Gorda. The community within this region most affected is Petrolia, at the confluence of the main and north forks of the Mattole River. There is neither a Flood Boundary and Floodway Map nor a Flood Insurance Rate Map for Petrolia, so here we make an example calculation of the impact on the flood plain boundary. The lowest topographic gradient, 1/140 (α = 0.41°), lies between the Mattole River and the west edge of town. The earthquake increased the topographic gradient by about 135 mm per km or 1/650 (β = 0.009°). At 21 m (70') above sea level, the flood plain boundary will shift to the north by about 62 m (200') toward Petrolia from the river bed. This is the largest expected change; where topographic gradients near Petrolia are steeper, the flood plain boundary change will be correspondingly smaller.

Sites Covered by Flood Boundary and Floodway Maps. The Flood Boundary maps closest to the zone of major earthquake deformation lie in the Eel river flood plain. The deformation gradients at the southern end of Panel 1120 of 1900 (Between Rio Dell and Rhonerville in the Eel River flood plain), are less than 1/133,500, and the topographic gradients ranges from 1/266 at Waddington to 1/100 at Fortuna. This results in flood plain boundary changes of just less than 1 m, much smaller than the uncertainty in the mapped boundary, and thus inconsequential.

Future Earthquake Hazards in Humboldt County

Tsunami Hazards. The 1992 earthquake ruptured the southernmost 15 km of a major fault known as the Cascadia subduction zone, which extends 200 km to the north. The earthquake excited a 0.5-m-high tsunami (seismic sea wave) at Crescent City, and a 0.25 m-high wave at North Spit, near Eureka [*Oppenheimer et al.*, 1993]. Because the earthquake struck at low tide, the tsunamis did no damage. A much larger compressional earthquake, however, such as an M=8.5 earthquake forecast for the entire Cascadia subduction zone [*Heaton and Hartzell*, 1986], could excite a tsunami of significantly greater height than produced by the Cape Mendocino shock. Not only would a large tsunami inundate communities along much of the Pacific Northwest coast minutes after the mainshock, but high water could persist for 8 hours at some localities.

Shaking Hazards. The Cape Mendocino earthquake sequence provides seismological and geodetic evidence that the motion between the offshore Gorda tectonic plate and the North America tectonic plate east of the Oregon and northern California coastline causes large compressional earthquakes on gently inclined 'thrust' faults: On these faults, the north American continent overrides the Pacific seafloor. In addition to the permanent ground motion and intense shaking generated by such shocks, the main shocks can trigger equally hazardous aftershock sequences on land. The 1992 mainshock ruptured only a small part of the plate boundary and apparently did not trigger slip on any of the recently active thrust faults observed onshore [*Clarke and Carver*, 1992]. Thus, given the high level of historical seismicity and emerging picture of many active faults, the region is likely to continue experiencing significant seismicity. Inspection of the integrity of engineered structures within Humboldt County would thus be a wise investment to promote the future safety and economic viability of the County.

References

Carver, G. A., A. S. Jayko, D. W. Valentine, W. H. Li, and A. Foss, Coastal uplift associated with the 1992 Cape Mendocino earthquakes, northern California, *Geology*, submitted, 1993.

Clarke, S. H., Jr., and G. A. Carver, Late Holocene tectonics and paleoseismicity, southern Cascadia subduction zone, *Science*, **255**, 188-192, 1992.

Dunklin, T. A., Shaking induced features resulting from the April, 1992 Cape Mendocino earthquake sequence: Implications for geomorphic evolution, *EOS, Transactions AGU, 1992 Fall Meeting Supplement*, 503, 1992.

Ekström, G., R. S. Stein, J. P. Eaton, and D. Eberhart-Phillips, Seismicity and geometry of a 110-km long blind thrust fault, 1, The 1985 Kettleman Hills, California, earthquake, *Journal of Geophysical Research*, **97**, 4843-4864, 1992.

Heaton, T. H., and Hartzell, S. H., Source characteristics of hypothetical subduction earthquakes in the northwestern United States, *Bulletin of the Seismological Society of America*, **76**, 675-708, 1986.

Marshall, G. A., R. S. Stein, and W. Thatcher, Faulting Geometry and slip from coseismic elevation changes: The 18 October 1989, Loma Prieta, California, earthquake, *Bulletin of the Seismological Society of America*, **81**, 1660-1693, 1991.

Oppenheimer, D., G. Beroza, G. Carver, L. Dengler, J. Eaton, L. Gee, F. Gonzalez, A. Jayko, W. H. Li, M. Lisowski, M. Magee, G. Marshall, M. Murray, B. Romanowicz, K. Satake, R. Simpson, P. Somerville, R. Stein, and D. Valentine, The Cape Mendocino, California, earthquakes of April 1992: Subduction at the triple junction, *Science*, **261**, 433-438, 1993 [reprinted in Appendix].

Stein, R. S., Discrimination of tectonic displacement from slope-dependent errors in geodetic leveling from southern California, 1953-1979, In D. W. Simpson and P. G. Richards (Eds.), *Earthquake Prediction—An International Review* (pp. 441-456). Maurice Ewing Series 4, AGU, 1981.

Appendix I

Annotated NGS Descriptions of Disturbed Bench Marks Listed in Table 6

(Sites subject only to groundwater withdrawal not included)

ACRN = LV0666 ********** BENCH MARK DESCRIPTION *********
DESIGNATION -- S 1401 STATE--CA COUNTY--HUMBOLDT
QUAD--0401241 QSN-- LATITUDE = N403042. LONGITUDE = W1240724.
MONUMENT BY--NGS YR--1988 MARK TYPE--VERTICAL CONTROL DISK
LAST RECOVERY BY--NGS YR--19920728 CONDITION--GOOD
STAMPING--S 1401 1988
***** SPECIFIC SETTING--ABUTMENT
***** MARK ORIGIN --- NGS
11.8 KM (7.35 MI) SOUTHERLY ALONG U.S. HIGHWAY 101 FROM THE JUNCTION OF THE NORTHWESTERN PACIFIC RAILROAD (FORTUNA OVERHEAD) IN FORTUNA, SET VERTICALLY IN THE NORTHEAST FACE OF THE NORTHWEST CONCRETE ABUTMENT OF A HIGHWAY BRIDGE SPANNING EEL RIVER, 5.1 M (16.7 FT) NORTHWEST OF THE EAST CORNER OF THE ABUTMENT, 4.7 M (15.4 FT) SOUTHEAST OF THE NORTHWEST END OF A CONCRETE GUARDRAIL, 3.6 M (11.8 FT) NORTHEAST OF THE CENTERLINE OF THE NORTHBOUND LANES OF THE HIGHWAY, 1.0 M (3.3 FT) BELOW THE LEVEL OF THE HIGHWAY, AND 0.9 M (3.0 FT) ABOVE THE GROUND SURFACE.

ACRN = LV0667 ********** BENCH MARK DESCRIPTION *********
DESIGNATION -- R 1401 STATE--CA COUNTY--HUMBOLDT
QUAD--0401241 QSN-- LATITUDE = N403030. LONGITUDE = W1240708.
MONUMENT BY--NGS YR--1988 MARK TYPE--VERTICAL CONTROL DISK
LAST RECOVERY BY--NGS YR--19920728 CONDITION--GOOD
STAMPING--R 1401 1988
***** SPECIFIC SETTING--ABUTMENT
***** MARK ORIGIN --- NGS
12.3 KM (7.65 MI) SOUTHERLY ALONG U.S. HIGHWAY 101 FROM THE JUNCTION OF THE NORTHWESTERN PACIFIC RAILROAD (FORTUNA OVERHEAD) IN FORTUNA, SET VERTICALLY IN THE NORTHEAST FACE OF THE SOUTHEAST CONCRETE ABUTMENT OF A HIGHWAY BRIDGE SPANNING EEL RIVER, 5.4 M (17.7 FT) SOUTHEAST OF THE NORTH CORNER OF THE ABUTMENT, 4.1 M (13.5 FT) NORTHWEST OF THE SOUTHEAST END OF A GUARDRAIL, 3.7 M (12.1 FT) NORTHEAST OF THE CENTER OF THE NORTHBOUND LANES OF THE HIGHWAY, 0.9 M (3.0 FT) BELOW THE LEVEL OF THE HIGHWAY, AND 0.9 M (3.0 FT) ABOVE THE GROUND SURFACE.

ACRN = LV0433 ********** BENCH MARK DESCRIPTION *********
DESIGNATION -- L 1086 STATE--CA COUNTY--HUMBOLDT
QUAD--0401242 QSN-- LATITUDE = N402726. LONGITUDE = W1240359.
MONUMENT BY--CGS YR--1967 MARK TYPE--BENCH MARK DISK
LAST RECOVERY BY--NGS YR--19920728 CONDITION--GOOD
STAMPING--L 1086 1967
***** SPECIFIC SETTING--BRIDGE GUARDRAIL
***** MARK ORIGIN --- CGS
20.7 KM (12.85 MI) SOUTHERLY ALONG U.S. HIGHWAY 101 FROM THE JUNCTION OF THE NORTHWESTERN PACIFIC RAILROAD (FORTUNA OVERHEAD) IN FORTUNA, IN TOP OF AND 0.3 M (1.0 FT) SOUTHEAST OF THE NORTHWEST END OF THE SOUTHWEST CONCRETE BRIDGE RAIL OF A HIGHWAY BRIDGE SPANNING THE EEL RIVER, 8.8 M (28.9 FT) SOUTHWEST OF THE CENTERLINE OF THE HIGHWAY,

AND 0.6 M (2.0 FT) ABOVE THE LEVEL OF THE HIGHWAY. NOTE--THE BRIDGE RAIL IS PART OF THE ABUTMENT.

11/16/93 USGS Inspection: Bridge span downwarped; steel span rammed abutment. Cracked concrete. Restraining cables tensioned on north; slack on south.

ACRN = LV0672 ********** BENCH MARK DESCRIPTION *********
DESIGNATION -- X 1401 STATE--CA COUNTY--HUMBOLDT
QUAD--0401242 QSN-- LATITUDE = N402719. LONGITUDE = W1240352.
MONUMENT BY--NGS YR--1988 MARK TYPE--VERTICAL CONTROL DISK
LAST RECOVERY BY--NGS YR--19920728 CONDITION--GOOD
STAMPING--X 1401 1988
***** SPECIFIC SETTING--ABUTMENT
***** MARK ORIGIN --- NGS
21.0 KM (13.05 MI) SOUTHERLY ALONG U.S. HIGHWAY 101 FROM THE JUNCTION OF THE NORTHWESTERN PACIFIC RAILROAD (FORTUNA OVERHEAD) IN FORTUNA, NEAR THE SOUTHWEST END OF THE SOUTHEAST CONCRETE ABUTMENT OF A HIGHWAY BRIDGE SPANNING THE EEL RIVER, 6.0 M (19.7 FT) NORTHWEST OF THE SOUTHEAST END OF A GUARDRAIL, 5.1 M (16.7 FT) SOUTHWEST OF THE CENTERLINE OF THE SOUTHBOUND LANES OF THE HIGHWAY, 0.6 M (2.0 FT) ABOVE THE LEVEL OF THE HIGHWAY, AND 0.1 M (0.3 FT) NORTHEAST OF THE SOUTHWEST FACE OF THE ABUTMENT.

11/16/93 USGS Inspection: Cables not tensioned at this end of bridge.

ACRN = LU1301 ********** BENCH MARK DESCRIPTION *********
DESIGNATION -- L 1085 STATE--CA COUNTY--HUMBOLDT
QUAD--0401233 QSN-- LATITUDE = N401715. LONGITUDE = W1235338.
MONUMENT BY--CGS YR--1967 MARK TYPE--BENCH MARK DISK
LAST RECOVERY BY--NGS YR--19920730 CONDITION--GOOD
STAMPING--L 1085 1967
***** SPECIFIC SETTING--RETAINING WALL
***** MARK ORIGIN --- CGS
0.1 KM (0.05 MI) NORTHEASTERLY ALONG SPROWEL CREEK ROAD FROM THE POST OFFICE IN GARBERVILLE, THENCE 0.5 KM (0.30 MI) NORTHERLY ALONG REDWOOD DRIVE, THENCE 30.0 KM (18.65 MI) NORTHERLY ALONG U.S. HIGHWAY 101, IN TOP OF AND 0.1 M (0.3 FT) NORTH OF THE SOUTH END OF A CONCRETE RETAINING WALL FOR A CATCH BASIN AT MILEPOST 29.99, 10.4 M (34.1 FT) EAST OF THE CENTERLINE OF THE NORTHBOUND LANES OF THE HIGHWAY, AND 1.4 M (4.6 FT) ABOVE THE LEVEL OF THE HIGHWAY.

ACRN = LU1298 ********** BENCH MARK DESCRIPTION *********
DESIGNATION -- J 1085 STATE--CA COUNTY--HUMBOLDT
QUAD--0401233 QSN-- LATITUDE = N401624. LONGITUDE = W1235239.
MONUMENT BY--CGS YR--1967 MARK TYPE--BENCH MARK DISK
LAST RECOVERY BY--NGS YR--19920730 CONDITION--GOOD
STAMPING--J 1085 1967
***** SPECIFIC SETTING--RETAINING WALL
***** MARK ORIGIN --- CGS
0.1 KM (0.05 MI) NORTHEASTERLY ALONG SPROWEL CREEK ROAD FROM THE POST OFFICE IN GARBERVILLE, THENCE 0.5 KM (0.30 MI) NORTHERLY ALONG REDWOOD DRIVE, THENCE 27.5 KM (17.10 MI) NORTHERLY ALONG U.S. HIGHWAY 101, NEAR THE SOUTHEAST END OF A CONCRETE RETAINING WALL FOR A CATCH BASIN AT MILEPOST 28.61, 10.7 M (35.1 FT) NORTHEAST OF THE CENTERLINE OF THE NORTHBOUND LANES OF THE HIGHWAY, AND 1.1 M (3.6 FT) ABOVE THE

LEVEL OF THE HIGHWAY.

ACRN = LU1299 ********** BENCH MARK DESCRIPTION *********
DESIGNATION -- K 1085 STATE--CA COUNTY--HUMBOLDT
QUAD--0401233 QSN-- LATITUDE = N401651. LONGITUDE = W1235308.
MONUMENT BY--CGS YR--1967 MARK TYPE--BENCH MARK DISK
LAST RECOVERY BY--NGS YR--19920730 CONDITION--GOOD
STAMPING--K 1085 1967
***** SPECIFIC SETTING--HEADWALL
***** MARK ORIGIN --- CGS
0.1 KM (0.05 MI) NORTHEASTERLY ALONG SPROWEL CREEK ROAD FROM THE POST OFFICE IN GARBERVILLE, THENCE 0.5 KM (0.30 MI) NORTHERLY ALONG REDWOOD DRIVE, THENCE 28.9 KM (17.95 MI) NORTHERLY ALONG U.S. HIGHWAY 101, NEAR THE CENTER OF THE EAST CONCRETE HEADWALL OF A CULVERT AT MILEPOST 29.30, 9.5 M (31.2 FT) EAST OF THE CENTERLINE OF THE NORTHBOUND LANES OF THE HIGHWAY, AND 0.3 M (1.0 FT) BELOW THE LEVEL OF THE HIGHWAY.

ACRN = LU1291 ********** BENCH MARK DESCRIPTION *********
DESIGNATION -- H 101 STATE--CA COUNTY--HUMBOLDT
QUAD--0401233 QSN-- LATITUDE = N401629. LONGITUDE = W1235058.
MONUMENT BY--CGS YR--1931 MARK TYPE--BENCH MARK DISK
LAST RECOVERY BY--NGS YR--19920729 CONDITION--GOOD
STAMPING--H 101 1931 228.143
***** SPECIFIC SETTING--CONCRETE POST
***** MARK ORIGIN --- CGS
0.1 KM (0.05 MI) NORTHEASTERLY ALONG SPROWEL CREEK ROAD FROM THE POST OFFICE IN GARBERVILLE, THENCE 0.5 KM (0.30 MI) NORTHERLY ALONG REDWOOD DRIVE, THENCE 10.3 KM (6.40 MI) NORTHERLY ALONG U.S. HIGHWAY 101, THENCE 16.6 KM (10.30 MI) NORTHERLY ALONG THE AVENUE OF THE GIANTS, 0.5 KM (0.30 MI) SOUTHEAST OF THE INTERSECTION OF A ROAD LEADING EAST TO EEL ROCK, 9.1 M (29.9 FT) EAST OF THE NORTHEAST END OF A PIPE CULVERT, 8.3 M (27.2 FT) NORTH OF UTILITY POLE NUMBER 5, 7.6 M (24.9 FT) NORTHEAST OF THE CENTERLINE OF THE AVENUE, 2.4 M (7.9 FT) ABOVE THE LEVEL OF THE AVENUE, 1.8 M (5.9 FT) SOUTHEAST OF AN EVERGREEN TREE, 0.4 M (1.3 FT) NORTHWEST OF A WITNESS POST, AND THE MONUMENT PROJECTS 0.05 M (0.16 FT) ABOVE THE GROUND SURFACE.

ACRN = LV0366 ********** BENCH MARK DESCRIPTION *********
DESIGNATION -- M 229 STATE--CA COUNTY--HUMBOLDT
QUAD--0401242 QSN-- LATITUDE = N402610. LONGITUDE = W1242403.
MONUMENT BY--CGS YR--1935 MARK TYPE--BENCH MARK DISK
LAST RECOVERY BY--NGS YR--19921007 CONDITION--GOOD
STAMPING--M 229 1935
***** SPECIFIC SETTING--PREFAB CONC. POST IN EARTH
***** MARK ORIGIN --- CGS
20.8 KM (12.90 MI) SOUTHEASTERLY ALONG MATTOLE ROAD FROM THE INTERSECTION OF CHAMBERS ROAD IN PETROLIA, IN A SMALL FLAT AREA ON THE SOUTH SLOPE OF A HILL, 45.0 M (147.6 FT) NORTH OF THE ROAD CENTERLINE, 41.0 M (134.5 FT) NORTH-NORTHEAST OF THE CENTER OF A GATE, 35.0 M (114.8 FT) NORTH OF A FENCE, 15.0 M (49.2 FT) ABOVE THE LEVEL OF THE ROAD, 0.3 M (1.0 FT) SOUTH OF A WITNESS POST, AND THE MONUMENT PROJECTS 0.1 M (0.3 FT) ABOVE THE GROUND SURFACE.

ACRN = LV0402 ********** BENCH MARK DESCRIPTION *********
DESIGNATION -- F 275 STATE--CA COUNTY--HUMBOLDT
QUAD--0401242 QSN-- LATITUDE = N402701. LONGITUDE = W1240825.
MONUMENT BY--CGS YR--1935 MARK TYPE--BENCH MARK DISK
LAST RECOVERY BY--NGS YR--19921017 CONDITION--GOOD
STAMPING--F 275 1935
***** SPECIFIC SETTING--PREFAB CONC. POST IN EARTH
***** MARK ORIGIN --- CGS
0.2 KM (0.10 MI) SOUTHEASTERLY ALONG WILDWOOD AVENUE FROM THE POST OFFICE IN RIO DELL, THENCE 7.9 KM (4.90 MI) SOUTHWESTERLY ALONG MONUMENT ROAD, 21.3 M (69.9 FT) SOUTHWEST OF TRIANGULATION STATION HPGN CA 01 07, 13.9 M (45.6 FT) EAST OF THE CENTER OF BEAR RIVER RIDGE ROAD, 10.0 M (32.8 FT) SOUTHWEST OF THE ROAD CENTER, 0.6 M (2.0 FT) ABOVE THE LEVEL OF MONUMENT ROAD, AND THE MONUMENT PROJECTS 0.2 M (0.7 FT) ABOVE THE GROUND SURFACE. NOTE--THE MONUMENT IS CHIPPED ON ALL SIDES, BUT IT IS SOLID IN PLACE.

ACRN = LV0362 ********** BENCH MARK DESCRIPTION *********
DESIGNATION -- H 229 STATE--CA COUNTY--HUMBOLDT
QUAD--0401242 QSN-- LATITUDE = N402934. LONGITUDE = W1241926.
MONUMENT BY--CGS YR--1935 MARK TYPE--BENCH MARK DISK
LAST RECOVERY BY--NGS YR--19921014 CONDITION--GOOD
STAMPING--H 229 1935
***** SPECIFIC SETTING--PREFAB CONC. POST IN EARTH
***** MARK ORIGIN --- CGS
0.3 KM (0.20 MI) SOUTHWESTERLY ALONG MAIN STREET FROM THE POST OFFICE IN FERNDALE, THENCE 0.1 KM (0.05 MI) NORTHWESTERLY ALONG OCEAN AVENUE, THENCE 15.6 KM (9.70 MI) SOUTHERLY ALONG MATTOLE ROAD, 5.8 M (19.0 FT) WEST OF THE SOUTH END OF A GATE, 5.4 M (17.7 FT) NORTH OF THE ROAD CENTERLINE, 0.4 M (1.3 FT) NORTH OF A FENCE, 0.3 M (1.0 FT) EAST OF A WITNESS POST, 0.3 M (1.0 FT) ABOVE THE LEVEL OF THE ROAD, AND THE MONUMENT PROJECTS 0.4 M (1.3 FT) ABOVE THE GROUND SURFACE.

ACRN = LV0243 ********** BENCH MARK DESCRIPTION *********
DESIGNATION -- C 1087 RESET STATE--CA COUNTY--HUMBOLDT
QUAD--0401241 QSN-- LATITUDE = N403702. LONGITUDE = W1241155.
MONUMENT BY--CADH YR--1970 MARK TYPE--BENCH MARK DISK
LAST RECOVERY BY--NGS YR--19920727 CONDITION--GOOD
STAMPING--C 1087 1967 RESET 1970
***** SPECIFIC SETTING--HEADWALL
***** MARK ORIGIN --- CADH
3.4 KM (2.10 MI) NORTHERLY ALONG U.S. HIGHWAY 101 FROM THE JUNCTION OF THE NORTHWESTERN PACIFIC RAILROAD (FORTUNA OVERHEAD) IN FORTUNA, IN TOP OF AND 0.2 M (0.7 FT) NORTHWEST OF THE SOUTHEAST END OF THE NORTHEAST CONCRETE HEADWALL OF A CULVERT AT MILEPOST 63.69, 19.8 M (65.0 FT) EAST OF THE CENTERLINE OF THE NORTHBOUND LANES OF THE HIGHWAY, AND 3.0 M (9.8 FT) BELOW THE LEVEL OF THE HIGHWAY.

ACRN = LV0237 ********** BENCH MARK DESCRIPTION *********
DESIGNATION -- Y 1086 STATE--CA COUNTY--HUMBOLDT
QUAD--0401241 QSN-- LATITUDE = N403532. LONGITUDE = W1240912.
MONUMENT BY--CGS YR--1967 MARK TYPE--BENCH MARK DISK
LAST RECOVERY BY--NGS YR--19920728 CONDITION--GOOD
STAMPING--Y 1086 1967
***** SPECIFIC SETTING--HEADWALL

***** MARK ORIGIN --- CGS
0.1 KM (0.05 MI) WESTERLY ALONG U.S. HIGHWAY 101 BUSINESS (MAIN STREET) FROM THE POST OFFICE IN FORTUNA, THENCE 0.8 KM (0.50 MI) NORTHERLY ALONG 12TH STREET, IN TOP OF AND 0.3 M (1.0 FT) NORTH OF THE SOUTH END OF THE EAST CONCRETE HEADWALL OF A CULVERT SPANNING ROHNER CREEK, 0.3 KM (0.20 MI) SOUTH OF FORTUNA HIGH SCHOOL, 0.2 KM (0.10 MI) NORTH OF THE INTERSECTION OF THE NORTHWESTERN PACIFIC RAILROAD, 12.2 M (40.0 FT) EAST OF THE CENTERLINE OF THE STREET, AND 1.4 M (4.6 FT) BELOW THE LEVEL OF THE STREET.

ACRN = LV0234 ********** BENCH MARK DESCRIPTION *********
DESIGNATION -- W 1086 STATE--CA COUNTY--HUMBOLDT
QUAD--0401241 QSN-- LATITUDE = N403415. LONGITUDE = W1240853.
MONUMENT BY--CGS YR--1967 MARK TYPE--BENCH MARK DISK
LAST RECOVERY BY--NGS YR--19920728 CONDITION--GOOD
STAMPING--W 1086 1967
***** SPECIFIC SETTING--HEADWALL
***** MARK ORIGIN --- CGS
4.0 KM (2.50 MI) SOUTHERLY ALONG U.S. HIGHWAY 101 FROM THE JUNCTION OF THE NORTHWESTERN PACIFIC RAILROAD (FORTUNA OVERHEAD) IN FORTUNA, IN TOP OF AND 0.3 M (1.0 FT) NORTH OF THE SOUTH END OF THE WEST CONCRETE HEADWALL OF PIPE CULVERT NUMBER 59.07, AND 11.6 M (38.1 FT) WEST OF AND LEVEL WITH THE CENTERLINE OF THE SOUTHBOUND LANES OF THE HIGHWAY.

ACRN = LV0429 ********** BENCH MARK DESCRIPTION *********
DESIGNATION -- G 1086 STATE--CA COUNTY--HUMBOLDT
QUAD--0401242 QSN-- LATITUDE = N402625. LONGITUDE = W1240130.
MONUMENT BY--CGS YR--1967 MARK TYPE--BENCH MARK DISK
LAST RECOVERY BY--NGS YR--19920728 CONDITION--GOOD
STAMPING--G 1086 1967
***** SPECIFIC SETTING--BRIDGE GUARDRAIL
***** MARK ORIGIN --- CGS
25.4 KM (15.80 MI) SOUTHERLY ALONG U.S. HIGHWAY 101 FROM THE JUNCTION OF THE NORTHWESTERN PACIFIC RAILROAD (FORTUNA OVERHEAD) IN FORTUNA, IN TOP OF AND 0.3 M (1.0 FT) EAST OF THE WEST END OF THE NORTH CONCRETE BRIDGE RAIL OF A HIGHWAY BRIDGE SPANNING GREENLOW CREEK, 6.4 M (21.0 FT) NORTH OF THE CENTERLINE OF THE NORTHBOUND LANES OF THE HIGHWAY, AND 1.1 M (3.6 FT) ABOVE THE LEVEL OF THE HIGHWAY.
NOTE--THE BRIDGE RAIL IS PART OF THE ABUTMENT.

11/16/93 USGS Inspection: Vertical crack in underside of south abutment.

ACRN = LU1485 ********** BENCH MARK DESCRIPTION *********
DESIGNATION -- Z 1085 STATE--CA COUNTY--HUMBOLDT
QUAD--0401233 QSN-- LATITUDE = N402350. LONGITUDE = W1235647.
MONUMENT BY--CGS YR--1967 MARK TYPE--BENCH MARK DISK
LAST RECOVERY BY--NGS YR--19920728 CONDITION--GOOD
STAMPING--Z 1085 1967
***** SPECIFIC SETTING--BRIDGE GUARDRAIL
***** MARK ORIGIN --- CGS
35.0 KM (21.75 MI) SOUTHERLY ALONG U.S. HIGHWAY 101 FROM THE JUNCTION OF THE NORTHWESTERN PACIFIC RAILROAD (FORTUNA OVERHEAD) IN FORTUNA, IN TOP OF AND 0.3 M (1.0 FT) NORTHWEST OF THE SOUTHEAST END OF THE SOUTHWEST CONCRETE BRIDGE RAIL OF AN OVERPASS (REDCREST EXIT), 9.1 M (29.9 FT) SOUTHWEST OF THE CENTERLINE OF THE SOUTHBOUND LANES OF THE

HIGHWAY, AND 1.1 M (3.6 FT) ABOVE THE LEVEL OF THE HIGHWAY. NOTE--THE BRIDGE RAIL IS PART OF THE ABUTMENT.

11/16/93 USGS Inspection: Cracking adjacent to bridge in pavement. Cement bridge guardrail repaired.

ACRN = LU1482 ********** BENCH MARK DESCRIPTION *********
DESIGNATION -- W 1085 STATE--CA COUNTY--HUMBOLDT
QUAD--0401233 QSN-- LATITUDE = N402237. LONGITUDE = W1235525.
MONUMENT BY--CGS YR--1967 MARK TYPE--BENCH MARK DISK
LAST RECOVERY BY--NGS YR--19920728 CONDITION--GOOD
STAMPING--W 1085 1967
***** SPECIFIC SETTING--HEADWALL
***** MARK ORIGIN --- CGS
38.2 KM (23.75 MI) SOUTHERLY ALONG U.S. HIGHWAY 101 FROM THE JUNCTION OF THE NORTHWESTERN PACIFIC RAILROAD (FORTUNA OVERHEAD) IN FORTUNA, NEAR THE EAST END OF THE NORTH CONCRETE HEADWALL OF THE HIGHWAY OVERPASS OF HIGH ROCK ROAD, AT MILEPOST 37.63, AND 10.1 M (33.1 FT) EAST OF AND LEVEL WITH THE CENTERLINE OF THE NORTHBOUND LANES OF THE HIGHWAY.

11/16/93 USGS Inspection: Bridge wing-wall offset; 10" of new asphalt.

ACRN = LU1304 ********** BENCH MARK DESCRIPTION *********
DESIGNATION -- P 1085 STATE--CA COUNTY--HUMBOLDT
QUAD--0401233 QSN-- LATITUDE = N401819. LONGITUDE = W1235359.
MONUMENT BY--CGS YR--1967 MARK TYPE--BENCH MARK DISK
LAST RECOVERY BY--NGS YR--19920730 CONDITION--GOOD
STAMPING--P 1085 1967
***** SPECIFIC SETTING--PIER
***** MARK ORIGIN --- CGS
0.1 KM (0.05 MI) NORTHEASTERLY ALONG SPROWEL CREEK ROAD FROM THE POST OFFICE IN GARBERVILLE, THENCE 0.5 KM (0.30 MI) NORTHERLY ALONG REDWOOD DRIVE, THENCE 32.7 KM (20.30 MI) NORTHERLY ALONG U.S. HIGHWAY 101, SET VERTICALLY IN THE WEST FACE OF THE FIRST CONCRETE PIER NORTH OF THE SOUTH ABUTMENT OF THE PESULA ROAD OVERPASS OF THE HIGHWAY, AT MILEPOST 31.61, 11.9 M (39.0 FT) SOUTH OF THE CENTERLINE OF THE SOUTHBOUND LANES OF THE HIGHWAY, 2.7 M (8.9 FT) SOUTH OF A GUARDRAIL, AND 1.0 M (3.3 FT) ABOVE THE LEVEL OF THE HIGHWAY.

11/16/93 USGS Inspection: Surfacial cracking along bridge and west end. fresh asphalt at ends of bridge.

ACRN = LU1302 ********** BENCH MARK DESCRIPTION *********
DESIGNATION -- M 1085 STATE--CA COUNTY--HUMBOLDT
QUAD--0401233 QSN-- LATITUDE = N401739. LONGITUDE = W1235333.
MONUMENT BY--CGS YR--1967 MARK TYPE--BENCH MARK DISK
LAST RECOVERY BY--NGS YR--19920730 CONDITION--GOOD
STAMPING--M 1085 1967
***** SPECIFIC SETTING--BRIDGE GUARDRAIL
***** MARK ORIGIN --- CGS
0.1 KM (0.05 MI) NORTHEASTERLY ALONG SPROWEL CREEK ROAD FROM THE POST OFFICE IN GARBERVILLE, THENCE 0.5 KM (0.30 MI) NORTHERLY ALONG REDWOOD DRIVE, THENCE 30.8 KM (19.15 MI) NORTHERLY ALONG U.S. HIGHWAY 101, IN TOP OF AND 0.3 M (1.0 FT) SOUTH OF THE NORTH END OF THE EAST

CONCRETE BRIDGE RAIL OF THE HIGHWAY OVERPASS OF WILLIFORD ROAD, AT MILEPOST 30.52, 9.1 M (29.9 FT) EAST OF THE CENTERLINE OF THE NORTHBOUND LANES OF THE HIGHWAY, AND 1.1 M (3.6 FT) ABOVE THE LEVEL OF THE HIGHWAY. NOTE--THE BRIDGE RAIL IS PART OF THE ABUTMENT.

11/16/93 USGS Inspection: Settling cracks in pavement to bridge.

ACRN = LU1280 ********** BENCH MARK DESCRIPTION *********
DESIGNATION -- X 1084 STATE--CA COUNTY--HUMBOLDT
QUAD--0401233 QSN-- LATITUDE = N401310. LONGITUDE = W1234835.
MONUMENT BY--CGS YR--1967 MARK TYPE--BENCH MARK DISK
LAST RECOVERY BY--NGS YR--19920729 CONDITION--GOOD
STAMPING--X 1084 1967
***** SPECIFIC SETTING--HEADWALL
***** MARK ORIGIN --- CGS
0.1 KM (0.05 MI) NORTHEASTERLY ALONG SPROWEL CREEK ROAD FROM THE POST OFFICE IN GARBERVILLE, THENCE 0.5 KM (0.30 MI) NORTHERLY ALONG REDWOOD DRIVE, THENCE 10.3 KM (6.40 MI) NORTHERLY ALONG U.S. HIGHWAY 101, THENCE 7.9 KM (4.90 MI) NORTHERLY ALONG THE AVENUE OF THE GIANTS, IN TOP OF AND 0.3 M (1.0 FT) WEST OF THE EAST END OF THE NORTH CONCRETE HEADWALL OF A PIPE CULVERT AT MILEPOST 4.79, 0.1 KM (0.05 MI) EAST OF THE INTERSECTION OF A PAVED ROAD LEADING EAST TO U.S. HIGHWAY 101, AND 5.5 M (18.0 FT) NORTH OF AND LEVEL WITH THE AVENUE CENTERLINE.

ACRN = LU1270 ********** BENCH MARK DESCRIPTION *********
DESIGNATION -- S 1084 STATE--CA COUNTY--HUMBOLDT
QUAD--0401233 QSN-- LATITUDE = N401004. LONGITUDE = W1234650.
MONUMENT BY--CGS YR--1967 MARK TYPE--BENCH MARK DISK
LAST RECOVERY BY--NGS YR--19920729 CONDITION--GOOD
STAMPING--S 1084 1967
***** SPECIFIC SETTING--HEADWALL
***** MARK ORIGIN --- CGS
0.1 KM (0.05 MI) NORTHEASTERLY ALONG SPROWEL CREEK ROAD FROM THE POST OFFICE IN GARBERVILLE, THENCE 0.5 KM (0.30 MI) NORTHERLY ALONG REDWOOD DRIVE, THENCE 8.6 KM (5.35 MI) NORTHERLY ALONG U.S. HIGHWAY 101, IN TOP OF AND 0.4 M (1.3 FT) SOUTHWEST OF THE NORTHEAST END OF THE SOUTHEAST CONCRETE HEADWALL OF A PIPE CULVERT AT MILEPOST 16.75, 18.9 M (62.0 FT) SOUTHEAST OF THE CENTERLINE OF THE NORTHBOUND LANES OF THE HIGHWAY, AND 1.3 M (4.3 FT) BELOW THE LEVEL OF THE HIGHWAY.

Reprint Series
23 July 1993, Volume 261, pp. 433–438

SCIENCE

The Cape Mendocino, California, Earthquakes of April 1992: Subduction at the Triple Junction

D. Oppenheimer, G. Beroza, G. Carver, L. Dengler, J. Eaton, L. Gee, F. Gonzalez, A. Jayko, W. H. Li, M. Lisowski, M. Magee, G. Marshall, M. Murray, R. McPherson, B. Romanowicz, K. Satake, R. Simpson, P. Somerville, R. Stein, and D. Valentine

The Cape Mendocino, California, Earthquakes of April 1992: Subduction at the Triple Junction

D. Oppenheimer, G. Beroza, G. Carver, L. Dengler, J. Eaton, L. Gee, F. Gonzalez, A. Jayko, W. H. Li, M. Lisowski, M. Magee, G. Marshall, M. Murray, R. McPherson, B. Romanowicz, K. Satake, R. Simpson, P. Somerville, R. Stein, D. Valentine

The 25 April 1992 magnitude 7.1 Cape Mendocino thrust earthquake demonstrated that the North America–Gorda plate boundary is seismogenic and illustrated hazards that could result from much larger earthquakes forecast for the Cascadia region. The shock occurred just north of the Mendocino Triple Junction and caused strong ground motion and moderate damage in the immediate area. Rupture initiated onshore at a depth of 10.5 kilometers and propagated up-dip and seaward. Slip on steep faults in the Gorda plate generated two magnitude 6.6 aftershocks on 26 April. The main shock did not produce surface rupture on land but caused coastal uplift and a tsunami. The emerging picture of seismicity and faulting at the triple junction suggests that the region is likely to continue experiencing significant seismicity.

On 25 April 1992 at 18:06 (UTC), a surface wave magnitude (M_s) 7.1 earthquake occurred near the town of Petrolia, California (Fig. 1). The main shock was followed the next day by two M_s 6.6 aftershocks at 07:41 and 11:41, located offshore about 25 km west-northwest of Petrolia. These three earthquakes and more than 2000 recorded aftershocks illuminated the configuration of the Mendocino Triple Junction, where the Pacific, North America, and southernmost Juan de Fuca (Gorda) plates meet. The occurrence of a M 7 earthquake is not unusual at the triple junction; over 60 earthquakes of Modified Mercalli intensity ≥ VI (*1*) or M ≥ 5.5 have occurred there since 1853 (*2*). However, this earthquake sequence may have provided the first direct evidence of interplate seismicity and thus impacts regional hazard assessment. In this article, we describe geophysical and seismological observations and discuss implications for seismic hazards in the Pacific Northwest.

Damage estimates ranged from $48 million to $66 million and President Bush declared the region a major disaster area. Much of the damage resulted from the main shock; however, fires triggered by the first large aftershock destroyed most of the Scotia shopping district, and both large, off-shore aftershocks caused additional structural damage. The relatively low incidence of injuries and structural damage caused by this sequence is primarily the result of low population density and the predominance of small, wood frame structures in the epicentral area. The sequence caused 356 reported injuries, destroyed 202 buildings, and caused damage to an additional 906 structures primarily in the towns of Petrolia, Ferndale, Rio Dell, Scotia, and Fortuna (Fig. 1) (*3*). It also triggered numerous landslides and rock falls and caused widespread liquifaction in local river valleys. Analysis of 1296 surveys in the north coast area indicate that the Modified Mercalli intensity peaked at IX in the Petrolia region and decreased in approximately a radial pattern around the epicenter (Fig. 1). Both of the two large aftershocks produced peak intensities of VIII, although the pattern was somewhat different from the main shock.

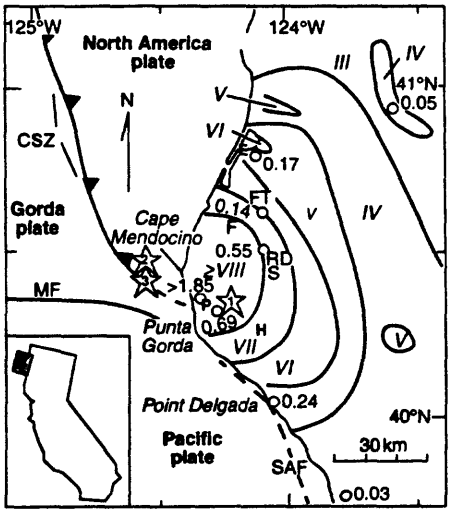

Fig. 1. Simplified tectonic map in the vicinity of the Cape Mendocino earthquake sequence. Stars, epicenters of three largest earthquakes; contours, Modified Mercalli intensities (values, Roman numerals) of main shock; open circles, strong motion instrument sites (*22*) (adjacent numbers give peak horizontal accelerations in *g*). Abbreviations: FT, Fortuna; F, Ferndale; RD, Rio Dell; S, Scotia; P, Petrolia; H, Honeydew; MF, Mendocino fault; CSZ, seaward edge of Cascadia subduction zone; and SAF, San Andreas fault.

Tectonic Setting

The Cape Mendocino earthquakes are a response to ongoing plate motions between the Gorda, North America, and Pacific plates at the Mendocino Triple Junction. The Gorda plate is converging on the North America plate at about 2.5 to 3 cm/year in the direction N50°E to N55°E (*4*). The seaward edge of Gorda plate subduction is marked by an abrupt change in sea-floor topography and by the western limit of the accretionary prism imaged in seismic reflection profiles (*5*). Active folds and thrust faults in Franciscan Complex and Cenozoic rocks and sediments of the overriding North America plate are parallel to the seaward edge of the Cascadia subduction zone (*6*).

Rigid plate theory predicts oblique convergence of the Gorda plate with the Pacific plate at 5 cm/year in the direction N115°E (*4*). Translational motion occurs along the east-west–trending, vertical, right-lateral Mendocino transform fault, whereas the convergence results in internal deformation of the Gorda plate. The attendant Gorda plate seismicity recorded in the 17 years before the Cape Mendocino sequence (*7*, *8*) (Fig. 2) has been concentrated in two parallel zones with a combined thickness of approximately 15 km. In the region of the Cape Mendocino earthquake, most seismic-

D. Oppenheimer, J. Eaton, A. Jayko, M. Lisowski, G. Marshall, M Murray, R. Simpson, and R. Stein are with the U.S. Geological Survey, Menlo Park, CA 94025. G. Beroza and M Magee are in the Geophysics Department, Stanford University, Stanford, CA 94305. G. Carver, L. Dengler, and R. McPherson are in the Department of Geology, Humboldt State University, Arcata, CA 95521. L. Gee and B. Romanowicz are at the University of California, Seismographic Station, ESB 475, Berkeley, CA 94720. F. Gonzalez is with the National Oceanic and Atmospheric Administration's Pacific Marine Environmental Laboratory, Seattle, WA 98115. W. H. Li is with Geological Sciences, AJ-20, University of Washington, Seattle, WA 98195. K. Satake is in the Department of Geological Sciences, University of Michigan, Ann Arbor, MI 48109. P. Somerville is with Woodward-Clyde Consultants, Pasadena, CA 91101 D. Valentine is in the Department of Geological Sciences, University of California, Santa Barbara, CA 93106

ity locates at depths greater than 17 km; the hypocenter zone dips about 6° eastward between 124.75° and 123.25°W, at which point the dip increases to about 25° (9). Most $M > 5$ earthquakes within the Gorda plate exhibit left-lateral motion on steep northeast-oriented faults (*7, 10*) that relieve convergence between the Gorda and Pacific plates through slip on preexisting planes of weakness inherited at the Gorda Ridge (*11*).

The San Andreas fault marks the principal Pacific–North America plate boundary south of the Mendocino Triple Junction. Triangulation data and observations of ground cracks indicate the fault ruptured as far north as Point Delgada in 1906 (*12*), but its location farther north is uncertain. Some studies place it immediately offshore (*13*), but others suggest that it merges with onshore faults at the triple junction (*5*). Geometry requires that the Pacific plate is also in contact with the North America plate along the Mendocino fault above the subducting Gorda plate.

Until the Cape Mendocino earthquake, few earthquakes were recorded with focal mechanisms that indicated slip on the Cascadia subduction zone. However, comparisons of the age, spreading rates, physiography, and seismicity of the Juan de Fuca–Gorda plate system with other subducting plates suggest that it does not subduct aseismically but instead is locked and capable of generating major earthquakes (*14*). Paleoseismic evidence of large, late Holocene subduction earthquakes is present along the subduction zone in submerged and buried wetlands (*15*), raised marine terraces (*16*), and surface displacement on thrust faults that may be genetically related to large subduction events (*17*). Radiocarbon dating indicates that at least three episodes of seismicity of similar age are represented in the stratigraphy from central Washington to northern California in the last 2000 years; the last episode occurred at about 1700 A.D. (*17*).

Observations

Seismicity. The hypocenter of the 25 April 1992 main shock was located 4 km east of Petrolia at a depth of 10.6 km (Fig. 3). A focal mechanism determined by the inversion of teleseismic mantle Rayleigh waves and aftershock locations indicate nearly pure thrust motion on a N10°W-striking fault plane that dips 13° to the east-northeast (*18*) (Table 1). The location of the hypocenter at the southeast end of the aftershock zone suggests that the fault ruptured unilaterally to the west (*19*). Most aftershocks <12 km deep (Fig. 3, circles) occurred within 10 km of the coast in a region bounded on the east by the mainshock epicenter, on the south by the Mendocino fault, and on the north by a west-northwest trend of earthquakes. The location, depth, and orientation of the rupture plane are consistent with the absence of surface faulting onshore.

The two M_s 6.6 aftershocks were located 30 km west of the main shock at depths near 20 km, and their mechanisms indicate right-lateral, strike-slip motion on planes striking to the southeast (*20*) (Fig. 3 and Table 1). The slip plane of the first after-

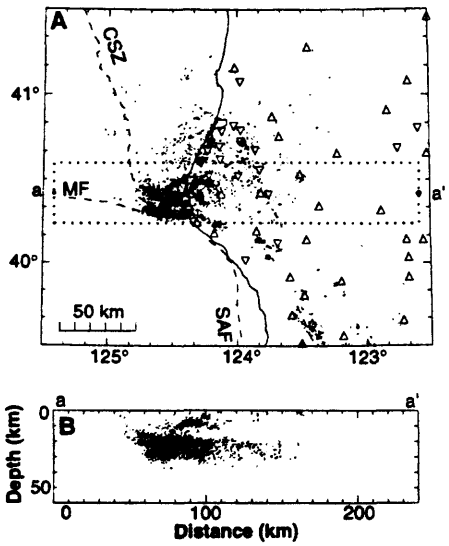

Fig. 2. Seismicity between August 1974 and time of main shock (*8*). (**A**) Locations of operating and discontinued seismic stations (upward and downward pointing triangles, respectively) at time of main shock. (**B**) Depths of earthquakes along cross section aa'. Depths west of longitude 124°40'W are unreliable. Note the gap in seismicity between main shock rupture plane at 10 km depth (Fig. 3B, aa') and pre–main shock seismicity at depths greater than 17 km. The earthquakes at cross section distance 200 km occur at depths greater than 35 km and begin to image the region of the Gorda plate where the dip increases. Earthquakes as deep as 90 km occur near longitude 122°10'W (*9*).

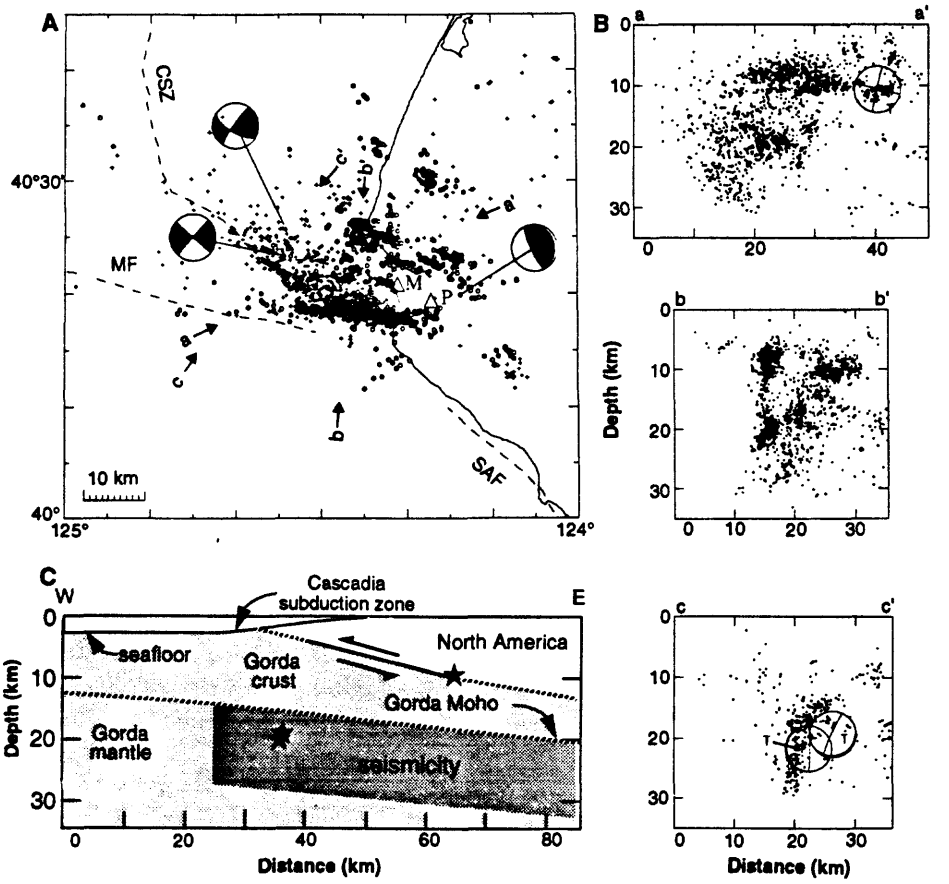

Fig. 3. (**A**) Focal mechanisms (lower hemisphere projections) of the main shock and two large aftershocks at their epicentral locations (compressional quadrants in black) and location of other aftershocks for 25 April 1992 to 30 September 1992 (circles for foci <12 km deep and plus symbols for deeper foci). (**B**) Depth of earthquakes on cross sections aa' (perpendicular to main shock strike, width ± 20 km), bb' (perpendicular to Mendocino fault, width ± 20 km), and cc' (perpendicular to strike of M_s 6.6 aftershocks, width ± 9 km). Compressional quadrant marked by "T." (**C**) East-west cross section depicts location of main shock rupture plane (solid line), hypocenters (stars), and pre–main shock seismicity with respect to plausible interpretation of Gorda–North America plate geometry.

shock is unknown because of the paucity of aftershocks. However, the second aftershock was located within a trend of smaller aftershocks at depths of 14 to 30 km on a southeast-striking plane that dips about 80° to the southwest (Fig. 3B, cc'); this orientation is consistent with the focal mechanism. The depths and mechanisms of the two large aftershocks provide evidence that rupture took place on faults in the Gorda plate, distinct from the main shock fault.

Although no large shocks ruptured the Mendocino fault during this sequence, many aftershocks occurred on the eastward projection of the fault (Fig. 3). The aftershock activity was bounded on the south where the distribution of hypocenters is near vertical and extends to a depth of 25 km (Fig. 3B, bb'). If this marks the boundary between the Gorda and Pacific plates, then the lack of any aftershocks in the Pacific plate suggests that the main shock represented strain release between the Gorda and North America plates. The mapped location of the Mendocino fault in this region is uncertain (5), and this east-west trend of seismicity may define the position of the Mendocino fault.

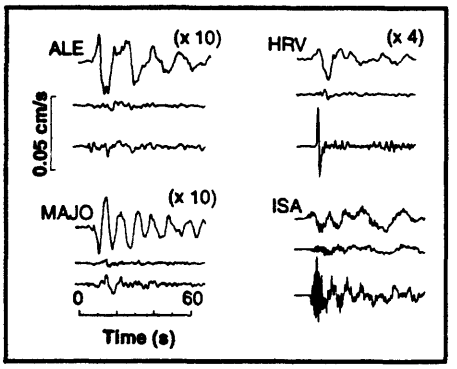

Fig. 4. Broad-band velocity records from four stations (ALE: epicentral distance Δ = 5185 km, azimuth = 9°; HRV: Δ = 4366 km, azimuth = 69°, MAJO: Δ = 8029 km, azimuth = 305°; ISA: Δ = 745 km, azimuth = 132°) for the main shock (top trace) and the first (middle) and second (lower) aftershocks. The amplitudes of the seismograms at ALE, HRV, and MAJO are increased relative to ISA for display. The large amplitudes of the second aftershock relative to the other two events in the along-strike azimuth (ISA) is attributable to rupture directivity.

Source properties. The mechanism and location of the two aftershocks were similar, but the second aftershock exhibited a strong variation of amplitude with azimuth (Fig. 4). The seismic moment of the second aftershock was approximately twice that of the first, but amplitudes of the P wave for this event were as much as 10 times as large near an azimuth of 130°. This variation is most easily attributable to enhancement of the amplitude in the direction of rupture, known as directivity (*21*). Directivity in P waves is surprising because it requires rupture velocities that are a large fraction of the P wave velocity. The high amplitudes and strong high-frequency content associated with the second aftershock may explain some of the differences in the intensity patterns for the main shock and two aftershocks. Although the second aftershock had 25% of the moment of the main shock, it has larger velocity amplitudes at stations to the southeast, such as ISA. The difference in both Modified Mercalli intensity and broad-band velocity records between the main shock and the second aftershock was probably enhanced by rupture propagation to the west during the main shock as inferred from the location of the hypocenter at the down-dip end of the rupture plane.

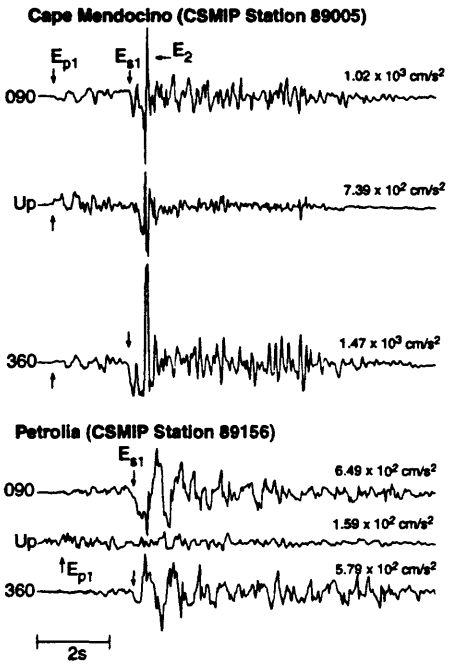

Fig. 5. Strong motion recordings and three components of the peak accelerations from stations of the California Strong Motion Instrumentation Program (CSMIP) at Cape Mendocino and Petrolia (*22*). Discernible first motion directions of the P and S waves for long-period event (E_{P1} and E_{S1}) are indicated, as is the large, high-frequency pulse at Cape Mendocino (E_2).

The strong ground motions of the main shock and two aftershocks were recorded on 14 instruments at epicentral distances of 5 to 130 km (Fig. 1), and the peak accelerations were some of the highest ever recorded (*22*). Recordings of the main shock at Petrolia and Cape Mendocino (Fig. 5) at epicentral distances of 5 and 10 km, respectively, have absolute time, facilitating the analysis of rupture evolution on the fault. Modeling of the large, long-period pulse that occurred 1 s after the main shock began (Fig. 5, E_{P1} and E_{S1}) with generalized ray theory indicates that this pulse originated from slip that occurred about 5 km up-dip from the hypocenter, beneath Petrolia. This result is consistent with the arrival times and polarities of the vertical P waves and horizontal S waves at both stations. In addition, the P wave first motions were upward and northwestward at Cape Mendocino. These motions indicate that the source was southeast of the station. This source location is consistent with the west-southwest direction of rupture determined from teleseismic surface waves (*19*), although that study inferred that the rupture initiated offshore. A large, high-frequency pulse (Fig. 5, E_2) followed the long-period pulse at Cape Mendocino and exceeded 1*g* on both horizontal components. This pulse was not discernible at the neighboring Petrolia station; thus, it cannot be explained simply by source effects but may represent motions that were generated or amplified locally near the Cape Mendocino station.

Table 1. Earthquake parameters.

	Origin time* (UTC)	Latitude* (North)	Longitude* (West)	Depth* (km)	Centroid depth† (km)	m_b‡	M_s‡	Moment† (dyn·cm)	Strike†	Dip†	Rake†
Main shock	25 April 18:06:05.16	40°19.94′	124°13.69′	10.6	20 to 25	6.3	7.1	4.45×10^{26}	349.7°	13.0°	105.6°
First aftershock	26 April 07:41:39.98	40°26.13′	124°34.43′	19.3	20 to 25	5.9	6.6	6.35×10^{25}	122.3°	75.9°	175.2°
Second aftershock	26 April 11:18:25.82	40°23.38′	124°34.30′	21.7	30 to 35	6.5	6.6	1.20×10^{26}	311.5°	89.6°	181.8°

*Hypocentral location determined from the local seismic network of the U.S. Geological Survey (*8*). †From surface-wave inversion (*18, 20*). ‡National Earthquake Information Center, Preliminary Determination of Epicenters.

Coseismic displacement. The elastic strain released by the main shock caused significant horizontal and vertical deformation in the epicentral region. The main shock elevated about 25 km of the coast from 3 km south of Punta Gorda to Cape Mendocino (Fig. 6). Many intertidal organisms inhabiting rocky reefs perished in the 3 weeks after the main shock. Maximum uplift was 140 ± 20 cm at Mussel Rock and 40 to 50 cm at the northernmost reef at Cape Mendocino (23). The lack of rocky intertidal environments farther north precluded the precise location of the northern limit of the uplift, but several near-shore rocks located about 7 km north of Cape Mendocino showed no evidence of uplift.

Coseismic horizontal and vertical site displacements in a regional geodetic network (Fig. 6) were determined from Global Positioning System (GPS) surveys in 1989, 1991, and 1 month after the main shock. The relative positions of most sites near the epicenter were measured shortly after the 17 August 1991 Honeydew earthquake [body wave magnitude (m_b) 6.0], which occurred 6 km south of the Cape Mendocino epicenter. The coseismic displacements were determined by comparison of the 1989 to 1992 observations, except in the vicinity of the Honeydew event where the 1991 survey was referenced. All displacements were corrected for secular strain accumulation estimated from Geodolite trilateration measurements made between 1981 and 1989. A site 13 km northeast of the epicenter had the largest measured coseismic displacement, moving 40 ± 2 cm to the west-southwest and subsiding 16 ± 8 cm.

Our preferred uniform-slip fault model (24), estimated from the coseismic site displacements and coastal uplift observations, indicates 2.7 m of nearly pure thrust motion occurred on a gently dipping fault plane. This model, chosen from a suite of acceptable models (24), is consistent with the main shock focal mechanism, the hypocenter location, and the distribution of aftershocks (Fig. 6 and Table 2). The range of geodetic moment inferred from the acceptable models is 2.5×10^{26} to 3.5×10^{26} dyn·cm, about 60% of the main shock seismic moment (Table 1). The model predicts a maximum uplift along the coast that is consistent with but somewhat less than the observed uplift. More complex models that use nonuniform slip to describe the rupture may improve these estimates of uplift and geodetic moment.

Table 2. Displacement model.

Parameter	Value
Width	16 km
Length	21.5 km
Depth to top edge	6.3 km
Latitude origin*	40°18.08'N
Longitude origin*	124°11.80'W
Depth at epicenter location	9.2 km
Moment†	2.79×10^{26} dyn·cm
Strike/dip/rake	350°/12.0°/94°
Slip	2.7 m

*Southeast corner of fault plane †Assumes uniform rigidity of 3×10^{11} dyn/cm^2

Tsunami. The main shock generated a small tsunami recorded by tide gauges along the California, southern Oregon, and Hawaii coastlines (Fig. 7). The largest tsunami amplitudes were recorded at Crescent City, California, where two well-defined packets of wave energy were recorded within the first 5 hours with maximum positive heights of 35 and 53 cm. Neither the precise arrival time nor the polarity of the first wave are clear because of the presence of background noise. However, the first packet of wave energy is consistent with the predicted travel time of 47 min for a wave ray path that traversed deep water. The second wave packet probably represents coastal trapped waves, or edge waves, having much slower velocities and amplitudes that rapidly decrease with distance offshore. Because the tsunami arrival nearly coincided with low tide at Crescent City, the wave did not cause any damage. The tsunami at Crescent City had an 8-hour duration; wave heights reached a maximum 3 to 4 hours after the first arrival. Tide gauges also recorded the initial arrival and subsequent edge waves at North Spit (Eureka, California) (20 min and 2.5 hours), Arena Cove (35 min and 3.5 hours), and Point Reyes (65 min and 3 hours).

Motion on the Plate Boundary

Interplate main shock. The main shock fault projects to the sea floor within 5 km of the seaward edge of the Cascadia subduction zone (25) (Fig. 3), suggesting that the main shock ruptured the Gorda–North America plate boundary. In contrast, the upper boundary of the pre–main shock seismicity, which is 7 km deeper than the main shock rupture plane (Figs. 2 and 3), projects to the surface about 85 km west of the Cascadia subduction zone and thus does not appear to define the plate boundary. The seismicity gap between the slip plane of the main shock and the pre–main shock seismicity is about the same thickness as the Gorda crust and overlying accretionary sediments, as determined from refraction experiments 10 km east of the seaward edge of the subduction zone (26). The gap may reflect a ductile subducted Gorda crust, and the inception of seismicity at a depth of 17 km may reflect brittle behavior of the Gorda upper mantle (27). Tabor and Smith (28) reached a similar conclusion from their observations of seismicity and velocity structure of the Juan de Fuca plate beneath the Olympic peninsula of Washington.

However, an inversion for the three-dimensional velocity structure of the region indicates that velocities typical of Gorda crust are evident at depths greater than 15 to 20 km (29). Moreover, modeling of

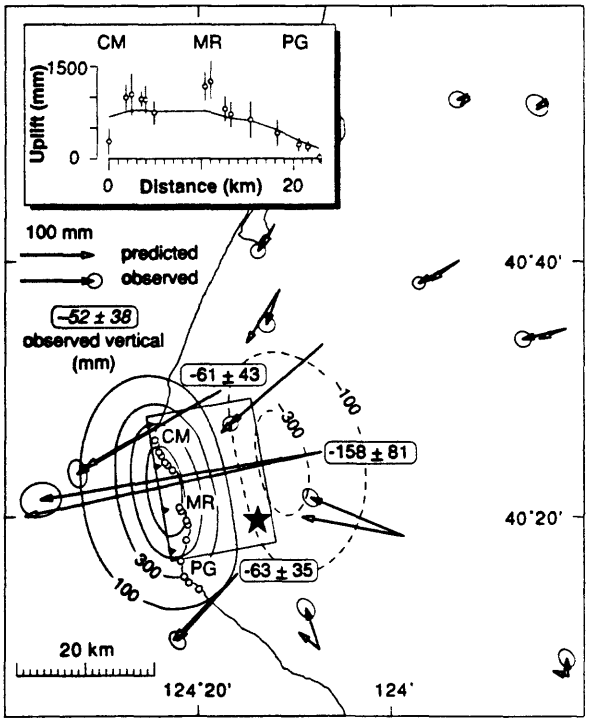

Fig. 6. Observed and predicted coseismic displacements for the Cape Mendocino main shock (epicenter located at star). The vectors are horizontal displacements relative to a site located at 41°9.20'N, 123°52.92'W. Observed displacements derived from GPS and Geodolite measurements; ellipses enclose regions of 95% confidence. Predicted displacements are from a model of uniform slip on the northeast-dipping rectangular fault plane, indicated by its surface projection. Rounded rectangles show vertical displacements measured by GPS that are greater than their standard deviations. Contours are elevation changes in millimeters predicted by the model. Abbreviations: CM, Cape Mendocino; MR, Mussel Rock; and PG, Punta Gorda. (**Inset**) Uplift measurements and their standard deviations from the die-off of marine organisms at coastal sites (open circles on map) and predicted uplift projected along N10°W.

thermal effects on the strength of the subducting oceanic lithosphere (30) suggests that the double seismic layers observed at depths of 20 and 30 km (Fig. 2) reflect, respectively, the brittle upper crust and upper mantle of the Gorda plate; the intervening, relatively aseismic region would correspond to the ductile lower crust. Consequently, these studies suggest that the Cape Mendocino main shock was an intraplate event in the North America plate.

Whether the main shock was an inter- or intra-plate event, the Cape Mendocino main shock clearly relieved strain resulting from the relative Gorda–North America plate motion. We note, however, that the main shock ruptured a region of the plate boundary that differs considerably from the boundary farther north, as indicated by the change in its orientation from north-northwest to northwest (5), the relatively narrow width of the plate, the likely presence of subducted sediments in the region of main shock rupture, and its younger age (4). Thus, this earthquake may not be typical of other Cascadia subduction zone earthquakes.

Intraplate aftershocks. The location, depth, and focal mechanisms of the two large aftershocks indicate that they ruptured the Gorda plate. The seismic data indicate that right-lateral slip occurred on a vertical, northwest-oriented fault plane for at least the second event. For most earlier Gorda shocks, rupture occurred as left-lateral slip on a northeast-oriented plane, perhaps because this orientation may allow reactivation of normal faults formed at the Gorda spreading ridge (11). From a consideration of stress release, either orientation reduces north-south compressional stress and down-dip tension in the Gorda plate, but rupture of the northwest-oriented plane may have been favored because of the static stress changes imposed by the main shock and, perhaps, the first aftershock.

To test this hypothesis, we modeled the changes in static stress (31) imposed by the main shock (Table 2) on three vertical fault planes: the east-west–oriented Mendocino fault, the possible N40°E-oriented slip plane of the first large aftershock, and the N50°W-oriented fault of the second large Gorda aftershock. Large regions of the northwest-oriented fault and the Mendocino fault received an increase in right-lateral shear stress greater than 3 bars and equally large increases in normal extension resulting from the main shock. Both the increase in right-lateral shear and the increased extension would bring both of these right-lateral faults closer to failure under a Coulomb failure criterion for nonzero coefficients of friction. About 90% of the aftershocks within 4 km of the Mendocino fault and the northwest Gorda fault occur where the modeling predicts the stress changes should load these faults toward failure for coefficients of friction ranging from 0.0 to 0.75. Thus, static stress changes may have helped trigger aftershocks along these two faults.

The model also indicates that static stress changes induced by the main shock are slightly more favorable for failure on a northeast-striking, left-lateral fault plane in the location of the first large aftershock, primarily because of a decrease in normal stress. In consideration of the present relative hypocentral locations of the two large aftershocks, slip on the northeast-oriented plane of the first aftershock would have added minor left-lateral shear to the northwest-oriented plane of the second aftershock but would have greatly decreased the normal stress on this plane. This scenario provides a simple mechanism in which the first aftershock helped trigger the second, similar to the scenario proposed for the Elmore Ranch–Superstition Hills pair of earthquakes (32).

Hazard implications. The Cape Mendocino earthquake sequence provided seismological evidence that the relative motion between the North America and Gorda plates results in significant thrust earthquakes. In addition to the large ground motions generated by such shocks, they can trigger equally hazardous aftershock sequences offshore in the Gorda plate and on the Gorda-Pacific plate boundary. This sequence illustrates how a shallow thrust event, such as the one of moment magnitude (M_w) 8.5 that is forecast for the entire Cascadia subduction zone (14), could generate a tsunami of greater amplitude than the Cape Mendocino main shock. Not only would this tsunami inundate communities along much of the Pacific Northwest coast within minutes of the main shock, but it could persist for 8 hours at some locales. The 25 April 1992 main shock ruptured only a small part of the plate boundary and apparently did not trigger slip on any of the Holocene shallow thrust faults observed onshore in the triple junction region (17). Thus, given the high level of historical seismicity and the emerging picture of many active faults, the region is likely to continue experiencing significant seismicity.

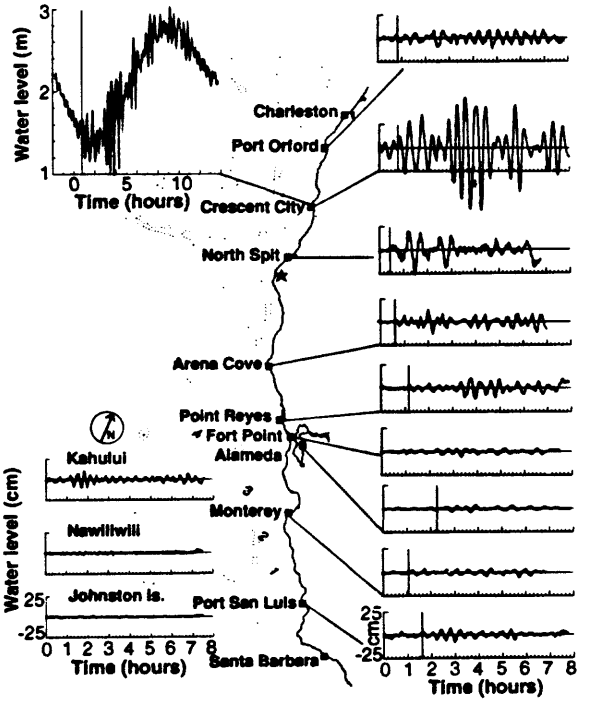

Fig. 7. Tsunami measurements at tide gauge stations along the coasts of California, Oregon, Hawaii, and Johnston Island. Tidal signal has been removed from all data except for Crescent City, California (inset) (note change of scale). Time of main shock is 0 hours. The vertical line marks the expected tsunami arrival time. Contour lines (dotted) represent ocean depth in kilometers, except for the single, unlabeled 500-m bathymetric contour line nearest the coast.

REFERENCES AND NOTES

1. H. O. Wood and F. Neumann, *Bull. Seismol. Soc. Am.* **21**, 277 (1931).
2. L. Dengler, G. Carver, R. McPherson, *Calif. Geol.* **45**, 40 (1992).
3. California Office of Emergency Services Situation Report, 4 May 1992; American Red Cross Disaster Update, 8 May 1992.
4. R. Riddihough, *J. Geophys. Res.* **89**, 6980 (1984); C. Nishimura, D. S. Wilson, R. N. Hey, *ibid.*, 10283, D. S. Wilson, *ibid.*, in press.
5. S. H. Clarke, Jr., *Am. Assoc. Pet. Geol. Bull.* **7**, 199 (1992).
6. H. M. Kelsey and G. A. Carver, *J. Geophys. Res.* **93**, 4797 (1988).
7. R. C. McPherson, thesis, Humboldt State University (1989).
8. Earthquakes for the period August 1974 to December 1984 were recorded by the Tera Corporation. Since 1983, the seismicity has been recorded by local networks operated by the U.S. Geological Survey and the University of California at Berkeley. All earthquake locations are based on a one-dimensional velocity model with station corrections developed from a joint hypocenter-velocity inversion of travel-time data and located with Hypoinverse [F. W. Klein, *U.S. Geol. Surv. Open File Rep. 89-314* (1989)]. Calibration explosions at Punta Gorda and Cape Mendocino were located to the northwest, 1.5 and 2.7 km, respe

tively, at the surface. Locations of the offshore earthquakes are not as accurate as those onshore because of the network geometry.
9. R. S. Cockerham, *Bull. Seismol. Soc. Am.* **74**, 569 (1984); S. R. Walter, *ibid.* **76**, 583 (1986).
10. T. V. McEvilly, *Nature* **220**, 901 (1968); J. P. Eaton, *Eos* **82**, 959 (1981); T. J. Lay, J. W. Given, H. Kanamori, *Bull. Seism. Soc. Am.* **72**, 439 (1982).
11. D. S. Wilson, *J. Geophys. Res.* **94**, 3065 (1989).
12. A. C. Lawson, *Carnegie Inst. Washington Publ.* **87**, 54 (1908); W. Thatcher and M. Lisowski, *Eos* **68**, 1507 (1987).
13. J. R. Curray and R. D. Nason, *Geol. Soc. Am. Bull.* **78**, 413 (1967); L. Seeber, M. Barazangi, A. Nowroozi, *Bull. Seismol. Soc. Am.* **60**, 1669 (1970).
14. T. H. Heaton and H. Kanamori, *Bull. Seismol. Soc. Am.* **74**, 993 (1984); T. H. Heaton and S. H. Hartzell, *ibid.* **76**, 675 (1986).
15. B. F. Atwater, *Science* **236**, 942 (1987); M. E. Darienz and C. D. Peterson, *Tectonics* **9**, 1 (1990); A. R. Nelson, *Quat. Res.* **38**, 74 (1992); G. S. Vick, thesis, Humboldt State University (1989); D. W. Valentine, thesis, Humboldt State University (1992).
16. D. Merritts and W. B. Bull, *Geology* 17, 1020 (1989).
17. S. H. Clarke, Jr., and G. A. Carver, *Science* **255**, 188 (1992).
18. We inverted for the main shock source parameters using the formalism of B. Romanowicz and T. Monfret [*Ann. Geophys.* **4**, 271 (1986)] and the spherical-Earth model PREM [A. M. Dziewonski and D. L. Anderson, *Phys. Earth Planet. Inter.* **25**, 297 (1981)] to correct for propagation effects. Rayleigh waves with periods between 140 and 320 s from a global distribution of stations were sampled at 10 frequencies.
19. An analysis of broad-band surface waves indicates that the main shock ruptured to the southwest (azimuth = 230°) with the largest moment release beginning 5 km from and extending to 20 km offshore [C. J. Ammon, A. A. Velasco, T. Lay, *Geophys. Res. Lett.* **20**, 97 (1993)].
20. For the aftershocks, we computed path-dependent amplitude and phase corrections based on analysis of the main shock. The approach of path-dependent corrections is advantageous for use of data at regional distances as well as shorter periods [M Pasyanos and B Romanowicz, *Eos* **73**, 372 (1992)].
21. H. Benioff, *Calif. Div. Mines Geol. Bull* 171, 199 (1955), A. Ben Menahem, *Bull. Seismol. Soc. Am.* **51**, 401 (1961).
22. A. Shakal *et al.*, *Calif. Div. Mines Geol. Rep OSMS 92-05* (1992).
23. Where colonies of organisms were completely killed, the vertical range of the organisms represents a minimum measure of the uplift. On some reefs, only the upper parts of some colonies of plants and sessile animals, such as mussels, died. The vertical extent of mortality in these colonies provided the best basis for estimates of the amount of uplift. The mean and standard deviation of the vertical extent of mortality for each colony (Fig. 6, inset) is estimated from multiple measurements made by a laser total station with an instrument precision of 1 mm.
24. We assumed that slip is uniform on a rectangular, planar fault embedded in an elastic half space. We performed a Monte Carlo search of the parameters describing the geometry of the fault plane and, for each geometry, used the horizontal and vertical GPS and coastal-uplift data to estimate the magnitude and rake of the slip vector. The scatter of the residuals for the best fitting models, including our preferred model (Table 2), is 2.2 times the a priori observational errors. An F-ratio test indicates other models with residual scatter less than 2 6 times the a priori errors do not differ significantly from the best fitting models at the 95% confidence level
25. In the projections, we assumed that faults are planar, the ocean depth is 2.3 km at the seaward edge of the Cascadia subduction zone at the latitude 40°27'N, and the mean elevation of the seismic network is 0.9 km. Main-shock parameters are from Table 1. We assumed the upper boundary of the background Gorda seismicity dips 6° east at a depth of 17.5 km at the coordinates of the main shock hypocenter.
26. G. G. Shor, P. Dehlinger, H. K. Kirk, W. S. French, *J. Geophys. Res.* **73**, 2175 (1968); S. W. Smith, J. S. Knapp, R. C. McPherson, *ibid.* **98**, 8153 (1993).
27. W. P. Chen and P. Molnar, *ibid.* **88**, 4183 (1983); P. Molnar and P. England, *ibid.* **95**, 4833 (1990).
28. J. J. Tabor and S. W. Smith, *Bull. Seismol. Soc. Am.* **75**, 237 (1985).
29. D. Verdonck and G. Zandt, *Lawrence Livermore Natl. Lab. Rep. UCRL-JC-111629* (1992).
30. K. Wang and G. Rogers, *Eos* **73**, 504 (1992).
31. We estimated static stress changes caused by the main shock using a rectangular dislocation surface (Table 2) in an elastic half-space [Y. Okada, *Bull. Seismol. Soc. Am.* **82**, 1018 (1992)] to stimulate the earthquake rupture. The results of the model are insensitive to small variations in the assumed fault geometries or slip distributions, although the maximum values and spatial details of the stress fields are.
32. K. Hudnut *et al.*, *Bull. Seismol. Soc. Am.* **79**, 282 (1989).
33. We thank B. Ellsworth, C. Weaver, D. Wilson, and D. Merritts for reviews of the manuscript. The measurement of coastal uplift was supported by a grant from the Pacific Gas and Electric Company.